UNLV Theses, Dissertations, Professional Papers, and Capstones

8-1-2014

Numerical Simulations of Traffic Flow Models

Puneet Lakhanpal
University of Nevada, Las Vegas, lakhanpa@unlv.nevada.edu

Follow this and additional works at: https://digitalscholarship.unlv.edu/thesesdissertations

Part of the Applied Mathematics Commons, Mathematics Commons, and the Transportation Commons

NUMERICAL SIMULATIONS OF TRAFFIC FLOW MODELS

By

Puneet Lakhanpal

Bachelor of Technology – Electronics and Communication
Indian Institute of Technology, Guwahati
2009

Masters of Science – Electrical Engineering
University of Nevada, Las Vegas
2011

A thesis submitted in partial fulfillment
of the requirements for the

Master of Science – Mathematical Sciences

Department of Mathematical Sciences
College of Sciences
The Graduate College

University of Nevada, Las Vegas
August 2014

UNLV
UNIVERSITY OF NEVADA LAS VEGAS

THE GRADUATE COLLEGE

We recommend the thesis prepared under our supervision by

Puneet Lakhanpal

entitled

Numerical Simulations of Traffic Flow Models

is approved in partial fulfillment of the requirements for the degree of

Master of Science - Mathematical Sciences
Department of Mathematical Sciences

Monika Neda, Ph.D., Committee Co-Chair

Pushkin Kachroo, Ph.D., Co-Chair

Amei Amei, Ph.D., Committee Member

Hongtao Yang, Ph.D., Additional Committee Member

Yingtao Jiang, Ph.D., Graduate College Representative

Kathryn Hausbeck Korgan, Ph.D., Interim Dean of the Graduate College

August 2014

ABSTRACT

NUMERICAL SIMULATIONS OF TRAFFIC FLOW MODELS

by

Puneet Lakhanpal

⟨Dr. Monika Neda⟩, Examination Committee Co-Chair
Associate Professor of Mathematical Sciences
University of Nevada, Las Vegas

⟨Dr. Pushkin Kachroo⟩, Examination Committee Co-Chair
Professor of Electrical and Computer Engineering
University of Nevada, Las Vegas

Traffic flow has been considered to be a continuum flow of a compressible liquid having a certain density profile and an associated velocity, depending upon density, position and time. Several one-equation and two-equation macroscopic continuum flow models have been developed which utilize the fluid dynamics continuity equation and help us find analytical solutions with simplified initial and boundary conditions. In this thesis, the one-equation Lighthill Witham and Richards (LWR) model combined with the Greenshield's model, is used for finding analytical and numerical solutions for four problems: Linear Advection, Red Traffic Light turning into Green, Stationary Shock and Shock Moving towards Right. In all these problems, the numerical solutions are computed using the Godunov Method and the Finite Element Method, and later they are compared to each other. Furthermore, the finite element time relaxation method is introduced for the treatment of the shocks in two numer-

ical problems : (a) Stationary Shock and (b) Shock moving towards the right. The optimal time relaxation parameters are numerically computed using three accuracy measures and finally, the effects of multiple time relaxation settings are explored.

ACKNOWLEDGEMENTS

TABLE OF CONTENTS

LIST OF TABLES

LIST OF FIGURES

CHAPTER 1

Introduction

Traffic flow can be defined as the study of how the vehicles move between origin and destination, and how the individual drivers interact with others. Since the driver behavior cannot be predicted with absolute certainity, mathematical models have been built which study the consistent behavior between the traffic streams via relationships such as flow q, density ρ and the mean velocity v. These mathematical models try to describe how these relationships evolve in space and time, and how they can be used to solve the real traffic flow conditions to be further used in traffic flow control and optimization (3). The Lighthill William and Richards (LWR) model is one such model that tries to capture the traffic behavior.

In this thesis, two tasks are explored.

1. Study of the LWR model with two techniques:

   - Finite Volume Godunov method

   - Finite Element Galerkin method with Time relaxation

2. Comparison of the solutions of following numerical problems with the above methods:

   - Linear Advection

   - A red traffic light turning into green

   - Stationary Shock

- Shock moving towards right

1.1 Outline of the Thesis

This thesis is divided into the following chapters.

1. Chapter 1 presents the motivation and outline of the thesis.

2. Chapter 2 presents a brief overview of the LWR traffic flow model and describes the speed-flow relationships.

3. Chapter 3 presents four problems in traffic flow for which numerical simulations are desired.

4. Chapter 4 presents the theory behind the Finite Volume Godunov method and the Finite Element method with time relaxation. These two methods will be cross-evaluated and their performance will be measured against each numerical problem.

5. Chapter 5 presents the numerical results obtained for each problem using Godunov and Finite Element method.

6. Chapter 6 presents the conclusion and outlines the areas of further research.

CHAPTER 2

Traffic Flow

2.1 Introduction

If a vehicle is assumed to be a molecule, then the traffic can be defined to be an incompressible fluid which cannot be compressed after a certain density. In 1955 and 1956, Lighthill, Whittam and Richards proposed a macroscopic traffic flow model, which is very popularly known as the LWR model. According to this model, the traffic flow was represented using a first order partial differential equation and was based on a hyperbolic system of conversation laws, as defined below.

2.1.1 Conservation Laws

A conservation law is a Partial Differential Equation of the form

$$\frac{\partial \rho}{\partial t} + \frac{\partial f}{\partial x} = 0 \tag{2.1}$$

where t represents the time coordinate; x represents the space coordinate, $\rho : \mathbb{R} \times \mathbb{R} \to \mathbb{R}^m$ is an m dimensional vector of conserved quantities and $f : \mathbb{R}^m \to \mathbb{R}^m$ reprents the *flux* or the rate of flow of the conserved quantity ρ. Furthermore, the flux in a given direction represents the amount of ρ which has crossed a unit surface in the given direction per unit time.

The system (2.1) is said to be hyperbolic if for each value of ρ, the eigen values of the Jacobian matrix $f'(\rho)$ are real and there exists a complete set of m linearly

independent eigen vectors, representing the diagonalizability of the matrix.

2.1.2 Traffic Flow Theory

The Traffic flow theory is the study of following three variables.

1. Density $\rho(x,t)$: Number of cars per unit distance, per lane.

2. Velocity $v(x,t)$

3. Traffic Flow $Q(x,t)$: Average number of cars passing per unit time, per lane.

The relationship between the above three variables is presented in the following sub-section.

Relationship between Traffic Flow variables

Let $\rho(x,t)$ and $V(x,t)$ be continuous functions of x and t. Consider a very small time interval Δt. During this small time interval, the values of $\rho(x,t)$ and $V(x,t)$ be approximated by constants. Therefore, during the time Δt, $V(x,t)\Delta t$ cars exist in the space as shown in Figure 2.1. Therefore, the number of cars passing an observer can be written as $V(x,t)\Delta t p(x,t)$. Hence, by definition,

$$Q(x,t) = p(x,t)V(x,t) \tag{2.2}$$

In 3-d space, the relationship $V = \dfrac{Q}{\rho}$ has been described in Gerlough and Huber (4) and can be illustrated in Figure 2.2
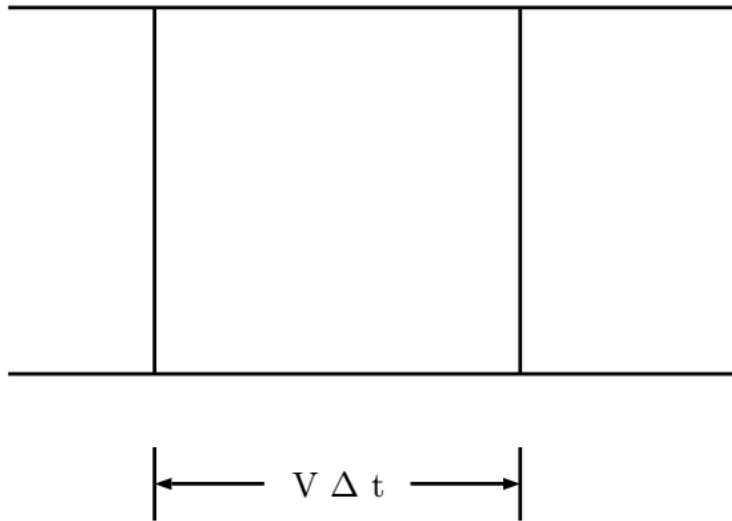
Figure 2.1: Distance travelled in Δt hours
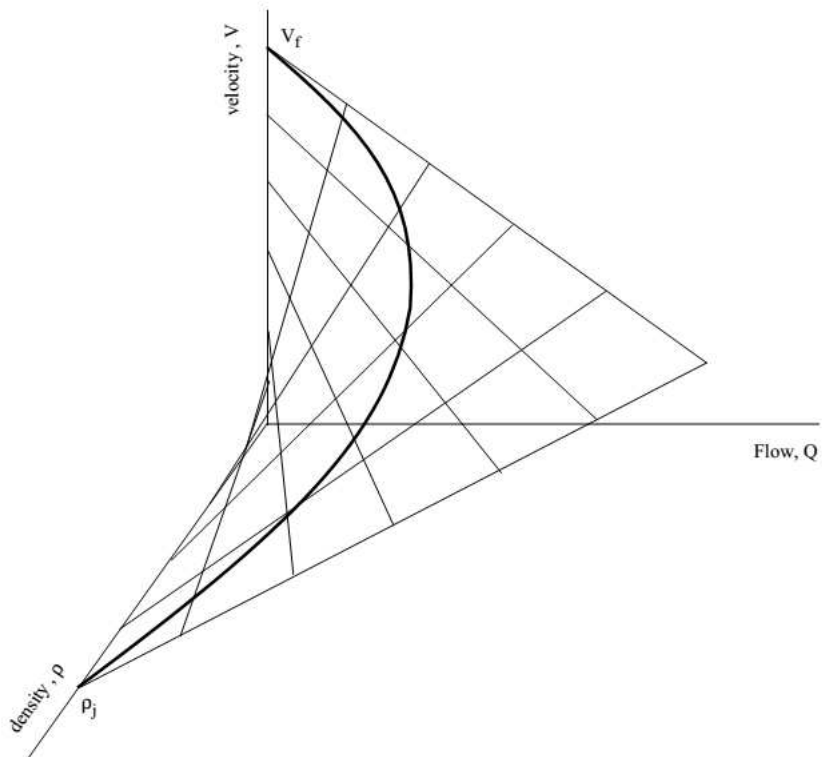
Figure 2.2: $v = \dfrac{Q}{\rho}$ represents the surface of admissible traffic flow model, where ρ_j represents the jam density and V_f represents the free-flow velocity (Source: Huber (4)).

CHAPTER 3

Problem Description

3.1 Introduction

In this chapter, we consider the one-equation Lighthill William and Richards (LWR) model of traffic flow, which will be used in conjunction with the Greenshield's model. Both these models formulate the basis of the numerical simulations in this thesis. Later, different variations of the LWR model will be used to define several well known numerical problems in the research literature.

3.2 LWR and Greenshield's model

The Lighthill-Whitham-Richards Model, commonly known as the LWR model, was introduced back in mid-1950s as a one dimensional macroscopic model to study the traffic flow. In this model, the traffic was considered to be an inviscid but compressible fluid (fluid-dynamic model) and the traffic flow variables: density ρ, velocity v and flow f, were defined as continuous variables in time and space. According to this model, the traffic flow f was defined to be a function of density ρ and *velocity* as shown in Equation (3.1)

$$\frac{\partial}{\partial t}\rho(t,x) + \frac{\partial}{\partial x}f(t,x) = 0 \qquad (3.1)$$

In Equation (3.1), ρ represents the traffic density of the vehicles which is related to the flux f and velocity v according to the relation $f = \rho v$, which was also introduced

6

in Equation (2.2).

Later, Greenshield's model connected the traffic density ρ and the traffic velocity v with a linear relationship illustrated in Equation (3.2).

$$v(\rho) = v_f \left(1 - \frac{\rho}{\rho_m} \right) \tag{3.2}$$

where v_f is the free flow speed and ρ_m is the maximum jam density. According to the Equation (3.2), the free flow speed v_f represents the speed of the traffic when the density ρ is zero. Similarly, the maximum density ρ_m is the traffic density at which speed of the traffic v is equal to zero. Due to the relation shown in Equation (3.2), the graph between the flux f and the density ρ assumes a concave shape, since $\frac{\partial^2 f}{\partial \rho^2} < 0$. This relationship is shown in Figure 3.1.

3.3   Numerical Problems

In this section, several well known numerical problems are defined as the variations of LWR and Greenshield's model. All these problems will later be numerically solved using the Godunov and Finite Element Method, as described in Chapter (4) and simulated in Chapter (5). This section defines the traffic flow PDE flow derived from Equations (3.1) and (3.2).

Considering the LWR and the Greenshield's model, we have
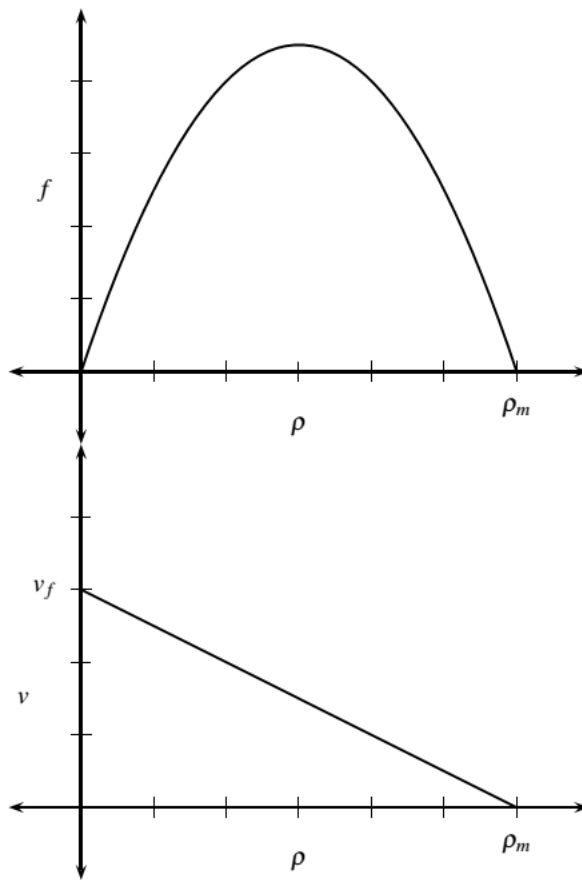
Figure 3.1: Experimental relationship between density, flow and velocity based on LWR and Greenshield's model (Source: Kachroo (9))

$$\frac{\partial}{\partial t}\rho(t,x) + \frac{\partial}{\partial x}f(\rho) = 0$$

$$f(\rho) = \rho v(\rho) \tag{3.3}$$

$$v(\rho) = v_f(1 - \frac{\rho}{\rho_m})$$

Replacing $v(\rho)$ in $f(\rho)$ and later $f(\rho)$ in the partial differential Equation (3.3), we get

$$\frac{\partial \rho}{\partial t} + \left(v_f - \frac{2v_f}{\rho_m}\rho\right)\frac{\partial \rho}{\partial x} = 0 \tag{3.4}$$

where the variables x, t have been suppressed with the notation definition that $\rho = \rho(x,t)$. Equation (3.4) is the general form of traffic flow PDE that will be used in this thesis.

3.3.1 Linear Advection

In Trangenstein (13), Linear Advection has been described as the motion of a conserved quantity along a constant velocity field. Therefore, contrary to the velocity being a function of density $v(\rho)$, the velocity assumes as constant speed c. This converts the equation (3.3) into,

$$\frac{\partial \rho}{\partial t} + c\frac{\partial \rho}{\partial x} = 0 \quad \forall x \in \Re \ \ \forall t > 0$$

$$\rho(x,0) = \rho_0(x) \quad \forall x \in \Re \tag{3.5}$$

The differential equation (3.5) can be re-written as follows,

$$0 = \begin{bmatrix} 1 & c \end{bmatrix} \begin{bmatrix} \dfrac{\partial \rho}{\partial t} \\[2ex] \dfrac{\partial \rho}{\partial x} \end{bmatrix} \tag{3.6}$$

In other words, the density gradient seems to be orthogonal to a constant vector. Therefore, the density ρ must be constant on lines parallel to the constant vector. These lines are called as characteristic lines, which in this case would be written as $x - ct = constant$. Hence,

$$\rho(x_0 + c\tau, t_0 + \tau) = constant \quad \forall(x_0, t_0) \ \forall \tau$$

If $\tau = t - t_0$ is chosen,

$$\rho(x_0 + c(t - t_0), t) = \rho(x_0 - ct_0, 0) = \rho_0(x_0 - ct_0)$$

If x is given, x_0 can be chosen such that $x_0 = x - ct + ct_0$ yields Equation (3.7), which will be the solution to the differential Equation (3.5).

$$u(x, t) = u_0(x - ct) \tag{3.7}$$

The statement that Equation (3.7) is the solution to the differential Equation (3.5) can be verified as below.

Define new variables ξ, τ and the corresponding density $\rho(\tilde{\xi}, \tau)$ such that

$$\xi = x - ct, \tau = t$$
$$\tilde{\rho}(\xi, t) = \rho(x, t) \tag{3.8}$$

If the chain rule is now applied to the system of equations (3.8), we get

$$
\begin{aligned}
\frac{\partial \rho}{\partial t} &= \frac{\partial \tilde{\rho}}{\partial \tau} - \frac{\partial \tilde{\rho}}{\partial \xi} c \\
\frac{\partial \rho}{\partial x} &= \frac{\partial \tilde{\rho}}{\partial \xi}
\end{aligned}
$$

Therefore, we get the following equation

$$
0 = \frac{\partial \rho}{\partial t} + c \frac{\partial \rho}{\partial x} = \frac{\partial \tilde{\rho}}{\partial \tau}
$$

$$
\tilde{\rho}(\xi, 0) = u_0(\xi)
$$

(3.9)

which proves that $\tilde{\rho}$ is the solution to the initial value problem defined in Equation (3.9).

Consider the initial profile of the density ρ in Equation (3.5) to have a discontinuity in the middle of a road segment, as shown in Figure 3.2. Therefore, provided that $c > 0$, the density ρ at time t will have the same profile, but only will be shifted $c * t$ units in space, as shown in Figure 3.3.
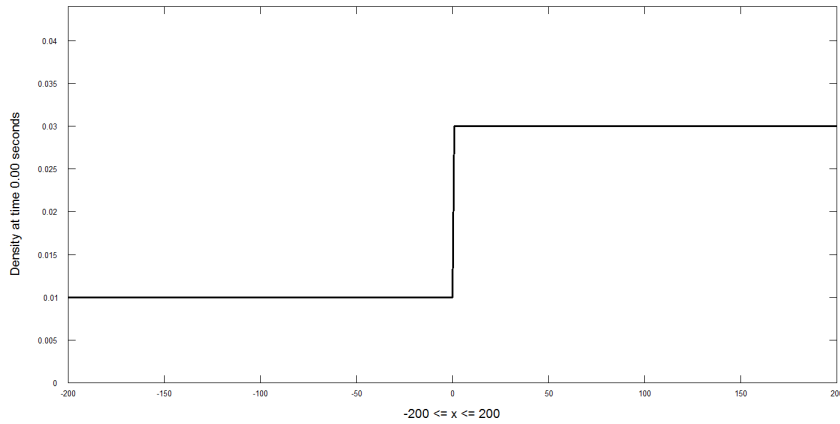
Figure 3.2: Linear Advection: Initial Density Profile $u_0(x)$

11
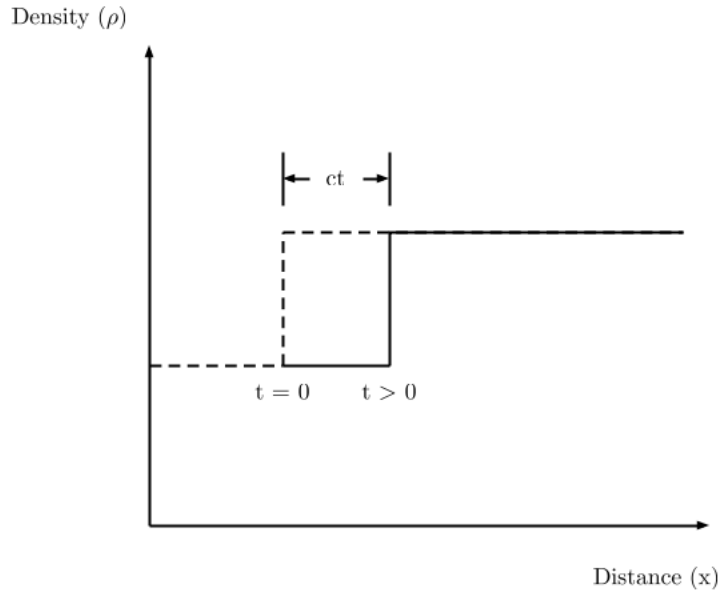
Figure 3.3: Linear Advection: Analytical solution of the Density Profile $u(x, t)$, given that $t > 0$ $c > 0$

3.3.2 Red Traffic Light Turning Into Green

Studying the behavior of how traffic density changes over time when a red traffic light turns into green, is a classic problem in traffic research. In this problem, it is assumed that a traffic light becomes red at time $t = 0$ such that the density behind the traffic light $\rho(x < 0; t = 0) = \rho_l$ becomes greater than the density ahead of the traffic light $\rho(x > 0; t = 0) = \rho_r$ further down the road. As a simpler case, it can also be assumed that the traffic behind the traffic light is lined up bumper to bumper such that $\rho(x < 0; t = 0) = \rho_m$. As an additional simplication, it can further be assumed that no traffic exists ahead of the traffic light further down the road such that $\rho(x > 0, t = 0) = 0$. However, let's study this problem in a general case when $\rho_l > \rho_r$.

The partial differential equation to be solved in this problem is as follows,

12

$$\frac{\partial \rho}{\partial t} + \left(v_f - \frac{2v_f}{\rho_m} \rho \right) \frac{\partial \rho}{\partial x} = 0$$

This equation was also introduced as Equation (3.4) earlier.

In quasilinear form, Equation (3.3) could be written as,

$$\frac{\partial}{\partial t} \rho(t, x) + f'(\rho) \frac{\partial}{\partial x} \rho(t, x) = 0 \tag{3.10}$$

From Equations (3.3) and (3.10), we get the characteristic speed as,

$$f'(\rho) = v_f (1 - 2\frac{\rho}{\rho_m}) \tag{3.11}$$

The characteristic speed obtained in Equation (3.11) is the slope of the graph shown in Figure 3.4.
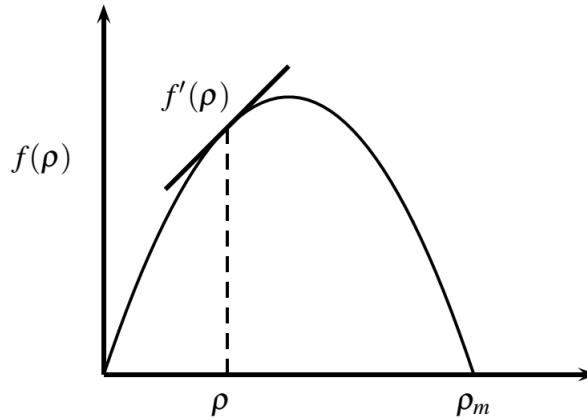
Figure 3.4: Characteristic speed (Source: Kachroo (9))

Following Equation (3.11), we observe that since $\rho_l > \rho_r$, therefore,

13

$$f'(\rho_l) = v_f(1 - 2\frac{\rho_l}{\rho_m}) < f'(\rho_r) = v_f(1 - 2\frac{\rho_r}{\rho_m}) \tag{3.12}$$

Since the characteristic speed towards the left of the traffic light is lesser than the characteristic speed towards the right, a blank region is created by these characteristics in the $x - t$ space. This behavior can be seen in Figure 3.5, as shown below.
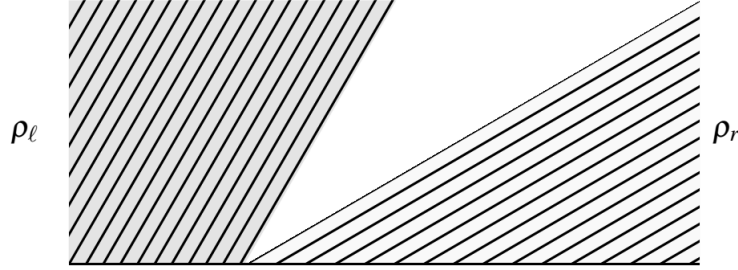
Figure 3.5: Red Light turning into Green: Characteristics generating blank region in $x - t$ space (Source: Kachroo (9))

In Kachroo (9), it has been mentioned that only a symmetry solution can fill in the gap as shown in Figure 3.5. Let's attempt to find such a solution.

Set $\rho(x, t) = w(x/t)$ and differentiate it with respect to time coordinate t and the space coordinate x. We get,

$$\begin{aligned}
\frac{\partial}{\partial t}\rho(x,t) &= -\frac{x}{t^2}w'(x/t) \\
\frac{\partial}{\partial x}\rho(x,t) &= \frac{1}{t}w'(x/t)
\end{aligned} \tag{3.13}$$

Substituting Equation (3.13) into Equation (3.10), we get

$$-\frac{x}{t^2}w'(x/t) + \frac{1}{t}f'\left(w(x/t)\right)w'(x/t) = 0 \tag{3.14}$$

If Equation (3.14) is multiplied by t and rearranged, it turns to Equation (3.15)

$$f'\left(w(\beta)\right)w'(\beta) = \beta w'(\beta) \tag{3.15}$$

Solving Equation (3.15), we get 2 cases:

Case I

$$w'(\beta) = 0 \tag{3.16}$$

i.e. w is a constant for $\beta \leq \beta_1$ and $\beta \geq \beta_2$.

Case II For $\beta_1 < \beta < \beta_2$, w varies smoothly with $w' \neq 0$. Therefore, Equation 3.15 yields Equation (3.17) as shown below.

$$f'\left(w(\beta)\right) = \beta \quad , \beta_1 < \beta < \beta_2 \tag{3.17}$$

Combining Case I and II, the density ρ becomes

$$\rho(\beta) = \begin{cases} \rho_l & , & \beta \leq f'(\rho_l) \\ w(\beta) & , & f'(\rho_l) < \beta f'(\rho_r) \\ \rho_r & , & \beta \geq f'(\rho_r) \end{cases} \tag{3.18}$$

Now, substituting back $w(x/t)$ by $\rho(x,t)$ in Equation (3.18), we get

$$\rho(x,t) = \begin{cases} \rho_l & , & \dfrac{x}{t} \leq f'(\rho_l) \\ \omega(\dfrac{x}{t}) & , & f'(\rho_l) < \dfrac{x}{t} \leq f'(\rho_r) \\ \rho_r & , & \dfrac{x}{t} \geq f'(\rho_r) \end{cases} \tag{3.19}$$

where

$$\omega(\frac{x}{t}) = \frac{f'(\rho_r) - f'(\rho_l)}{\rho_r - \rho_l}(\frac{x}{t})$$

The density solution, obtained in Equation (3.19), also known as a rarefaction solution, can be illustrated in Figure 3.6.
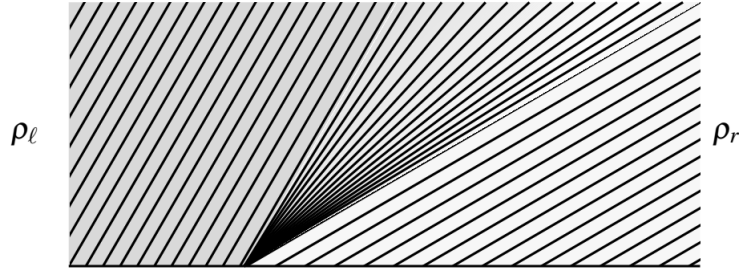
Figure 3.6: Red Light turning into Green: Rarefaction solution (Source: Kachroo (9))

3.3.3 Stationary Shock

A shock in density happens when the characteristics intersect in space and time. When characteristics intersect, that point in space has multiple values of densities at the same time. In this problem, the density behind a certain point on the road

16

segment (say $x = 0$) $\rho(x < 0; t = 0) = \rho_l$ is taken to be lesser than the density ahead of that point $\rho(x > 0; t = 0) = \rho_r$ further down the road. In other words, at time $t = 0$, $\rho_l < \rho_r$. As a special case, ρ_l can be taken to be 0 and ρ_r can be taken to be ρ_m. In this case, according to Haberman (5), the situation will be interpreted as an initial semi-infinite line of bumper to bumper traffic followed by no traffic.

The partial differential equation to be solved in this problem is defined in Equation (3.4). Additionally, the characteristic speed was also introduced as follows in Equation (3.11).

$$f'(\rho) = v_f(1 - 2\frac{\rho}{\rho_m})$$

For shocks in general, since $\rho_l < \rho_r$, therefore,

$$f'(\rho_l) = v_f(1 - 2\frac{\rho_l}{\rho_m}) > f'(\rho_r) = v_f(1 - 2\frac{\rho_r}{\rho_m}) \tag{3.20}$$

Based upon Equation (3.20), since the characteristic speed on the left $f'(\rho_l)$ is higher than that on the right $f'(\rho_r)$, therefore, the characteristic curves from the left catch up with those on the right. This produces a shock wave with speed λ given by *Rankine-Hugoniot* condition, as described in Kachroo (9). These characteristics are shown in Figure 3.7 and the shock speed is defined in Equation (3.21).

$$\lambda = \frac{f(\rho_r) - f(\rho_l)}{\rho_r - \rho_l} \tag{3.21}$$

A stationary shock is produced when ρl and ρ_r are chosen such that the shock

17
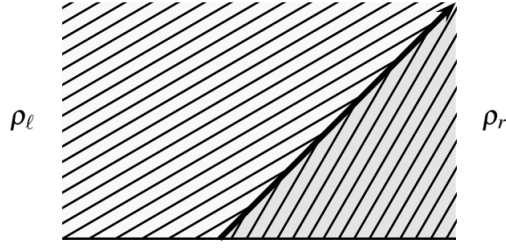
Figure 3.7: Shock solution and its characteristics (Source: Kachroo (9))

speed given by Equation (3.21) is 0. In other words, given an initial density profile

shown in Figure 3.8 and stated in Equation (3.22) , the shock stays at the same

position $\forall\, t > 0$, as shown in Figure 3.9 and stated in Equation (3.23).

$$\rho(x,0) = \begin{cases} \rho_l & x < a \\ \rho_r & x >= a \end{cases} \tag{3.22}$$

$$\rho(x,t) = \begin{cases} \rho_l & x < a \\ \rho_r & x >= a \end{cases} \tag{3.23}$$

3.3.4 Shock moving towards right

As introduced earlier in the previous subsection, a shock is formed when characteristics intersect at $t > 0$. This situation arises when $\rho_l < \rho_r$, thereby leading to $f'(\rho_l) > f'(\rho_r)$ as per Equation (3.20).

Additionally, the shock moves towards right if the shock speed defined in Equation (3.21) is positive. In other words, $\lambda > 0$ as per Equation (3.24).

Density $(\rho(x,0))$
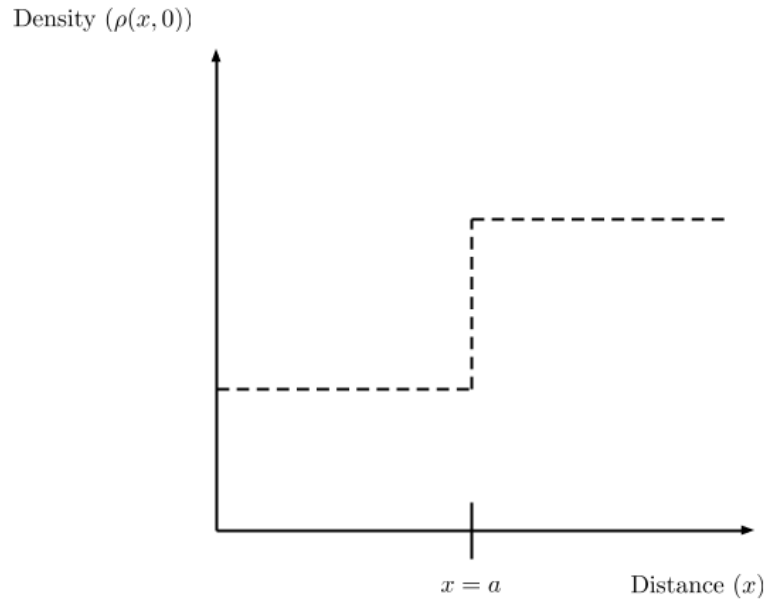
Figure 3.8: Stationary Shock: Initial Condition at time $t = 0$
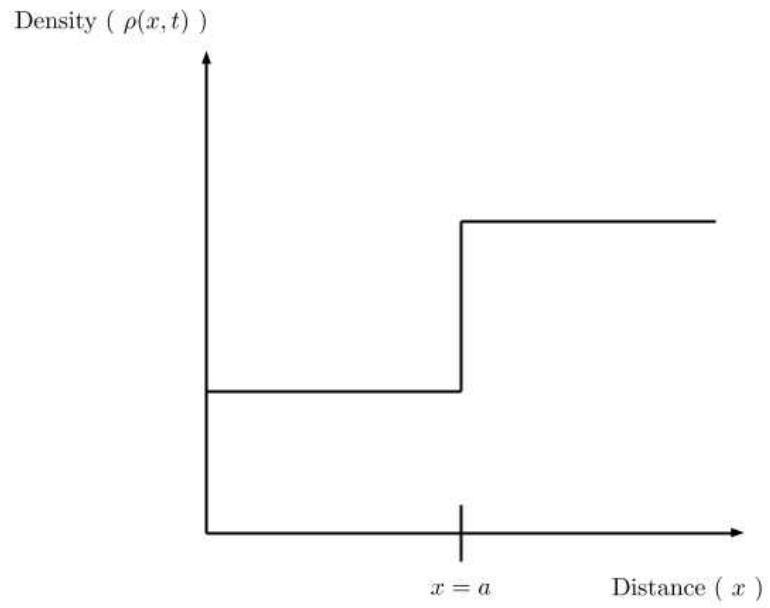
Density ($\rho(x,t)$)

Figure 3.9: Stationary Shock: Solution $\forall t$

$$\lambda = \frac{f(\rho_r) - f(\rho_l)}{\rho_r - \rho_l} > 0 \tag{3.24}$$

The partial differential equation to be solved in this problem is as follows,

$$\frac{\partial \rho}{\partial t} + v_f \frac{\partial \rho}{\partial x} - \frac{2v_f}{\rho_m} \rho \frac{\partial \rho}{\partial x} = 0$$

This equation was also introduced as Equation (3.4) earlier. The density profile at time $t = 0$ and $t > 0$ are shown in Figures 3.10 and 3.11 respectively.

Density $(\rho(x, 0))$

Distance (x)

$x = a$
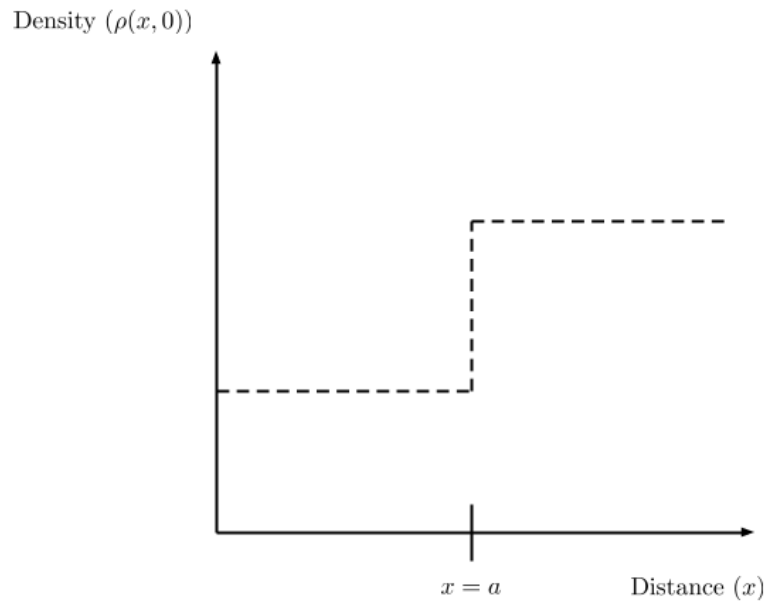
Figure 3.10: Shock moving towards right: Initial Condition at time $t = 0$
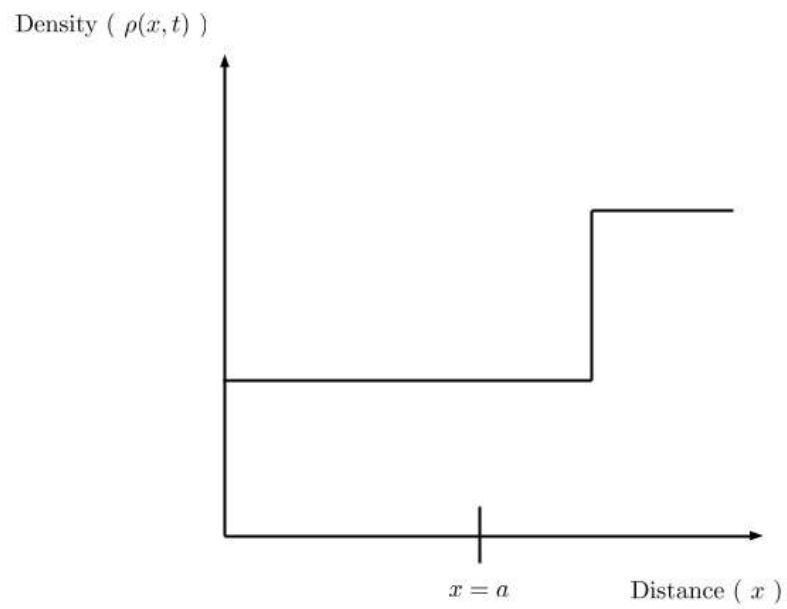
Figure 3.11: Shock moving towards right: Solution at time $t > 0$

CHAPTER 4

Numerical Methods

4.1   Introduction

In this chapter, the basics of two numerical methods are introduced - Godunov and Finite Element. Later, the Finite Element method is enhanced by introducing the concept of time relaxation in traffic flow.

4.2   Godunov method

This section provides the basics of the Godunov method and later specifies the Traffic Flow PDE being used in the Godunov analysis.

4.2.1   Basics of Godunov method

The Godunov method of numerical simulations is a conservative scheme, where the solution can be represented in the following form:

$$\rho_i^{n+1} = \rho_i^n + \frac{\Delta t}{\Delta x}[f_{i-\frac{1}{2}} - f_{i+\frac{1}{2}}] \tag{4.1}$$

where

$$f_{i+\frac{1}{2}} = f_{i+\frac{1}{2}}(\rho_{i-l_L}^n, \cdots, \rho_{i+l_R}^n) \tag{4.2}$$

with l_L and l_R being two non-negative integers and $f_{i+\frac{1}{2}}$ being a numerical approximation to the flux $f(\rho)$, as described in Equation (3.1).

This method is widely used for solving Riemann problems, as shown in Figure 4.1

and defined in Equation (4.3).
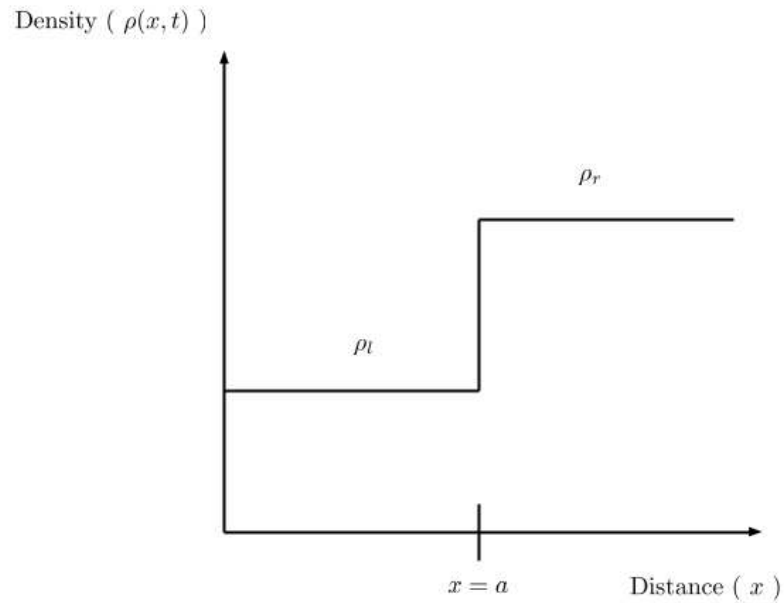
Figure 4.1: Definition Sketch for Riemann Problem

$$\rho(x, t = 0) = \begin{cases} \rho_l(x) & ; x \leq a \\ \rho_r(x) & ; x > a \end{cases} \qquad (4.3)$$

where ρ_l and ρ_r are two functions of coordinate x and a is the location of the initial discontinuity.

As introduced earlier, Equation (3.21) provides the speed of the shock wave, which exists when $\rho l < \rho r$. However, a rarefaction is obtained when $\rho_l > \rho_r$.

$$\lambda = \frac{f(\rho_r) - f(\rho_l)}{\rho_r - \rho_l}$$

This analysis of shockwave and rarefaction conditions provides us the Godunov

based ODE model for traffic. The conservation law of traffic flow allows us to create

this ODE model and is given in Equation (4.4).

$$\frac{\mathrm{d}\rho(t)}{\mathrm{d}t} = f_{in} - f_{out} + u(t) \tag{4.4}$$

where a unit length for the section is considered. This equation is derived from Figure

4.2, as shown below.
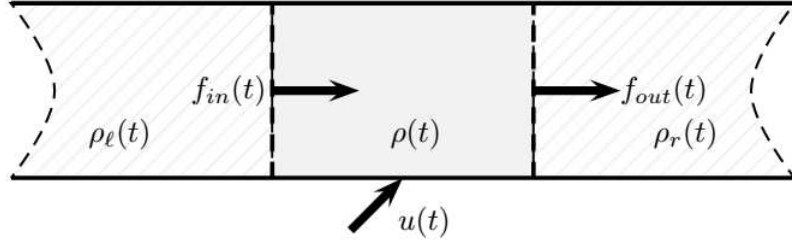
Figure 4.2: Godunov Dynamics (Source: Kachroo(12))

In the Figure 4.2, $f_{in}(t)$ represents the inflow, $f_{out}(t)$ represents the outflow, $\rho_l(t)$

represents the upstream density and $\rho_r(t)$ represents the downstream density at time

t. Using the function $F(.,.)$ obtained using the Godunov method (11) at the left

junction, the inflow $f_{in}(t)$ can be computed using Equation (4.5).

$$f_{in}(t) = F(\rho_l, \rho) \tag{4.5}$$

Similarly, for the right junction, the outflow $f_{out}(t)$ can be computed using Equa-

tion (4.6).

$$f_{out}(t) = F(\rho, \rho_r) \tag{4.6}$$

In Leveque (11), it has been mentioned that the function $F(\rho_l, \rho_r)$ can be written in terms of its arguments using the Godunov method as,

$$F(\rho_l, \rho_r) = f(\rho^*(\rho_l, \rho_r)) \tag{4.7}$$

where the term ρ^* represents the flow dictating density and is computed as follows,

1. $f'(\rho_\ell), f'(\rho_r) \geq 0 \Rightarrow \rho^* = \rho_\ell$

2. $f'(\rho_\ell), f'(\rho_r) \leq 0 \Rightarrow \rho^* = \rho_r$

3. $f'(\rho_\ell) \geq 0 \geq f'(\rho_r) \Rightarrow \rho^* = \rho_\ell$ if $\lambda > 0$, otherwise $\rho^* = \rho_r$

4. $f'(\rho_\ell) < 0 < f'(\rho_r) \Rightarrow \rho^* = \rho_\lambda$

Here, ρ_λ is obtained as the solution to $f'(\rho_\lambda) = 0$.

4.2.2 LWR-Greenshield's Traffic Flow PDE used in Godunov analysis

As introduced earlier in Equation (3.4), the following Traffic Flow PDE is used for numerical simulations using Godunov analysis.

$$\frac{\partial \rho}{\partial t} + \left(v_f - \frac{2v_f}{\rho_m} \rho \right) \frac{\partial \rho}{\partial x} = 0$$

The above definition of $F(\rho_l, \rho_r) = f(\rho^*(\rho_l, \rho_r))$ is used to compute the traffic density ρ, as defined earlier in Equation (4.1).

$$\rho_i^{n+1} = \rho_i^n + \frac{\Delta t}{\Delta x}[f_{i-\frac{1}{2}} - f_{i+\frac{1}{2}}]$$

4.3 Finite Element method

This section provides the basics of the Finite Element method, specifies the Traffic Flow PDE being used in the FEM analysis and later introduces the concepts of time relaxation important while treatment of shocks.

4.3.1 Basics of Finite Element method

According to Hutton (7), Finite Element Method (FEM) is a computational technique to obtain approximate solutions of boundary value problems, which are mathematical problems where one or more dependent variables satisfy a differential equation everywhere within a known domain and satisfy specific conditions on the boundary of the domain. In FEM, a small finite element of size $dx \times dy$ that encloses a finite-sized subdomain is first defined as shown in Figure 4.3(b). The vertices of the element are called as nodes, where the value of the dependent variable is explicity calculated for the finite element. At these nodes, the value of the dependent variables are first computed and then are used to approximate the values at non-nodal points by interpolating those nodal values. For instance, consider ϕ_1, ϕ_2 and ϕ_3 to be the nodal values of the dependent variable in Figure 4.3(b). Then, with the help of N_1, N_2 and N_3 interpolation (or shape) functions, the dependent variable within the element is
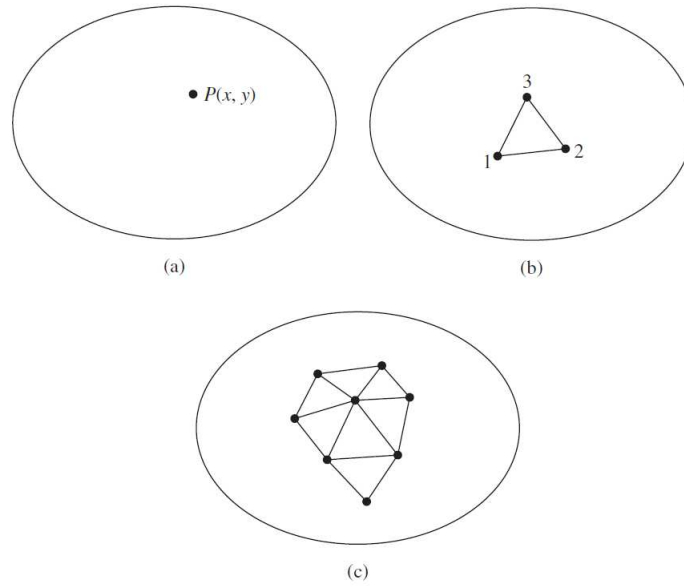
Figure 4.3: (a) $2-D$ domain of dependent variable $\phi(x,y)$ (b) Three node Finite Element defined in domain (c) Additional elements showing partial mesh of domain

defined by Equation (4.8).

$$\phi(x,y) = N_1(x,y)\phi_1 + N_2(x,y)\phi_2 + N_3(x,y)\phi_3 \qquad (4.8)$$

The triangulation element shown in Figure 4.3(b) and described in Equation (4.8) is said to have 3 degrees of freedom, since three nodal values are necessary to describe the dependent variable within the element. In general, degree of freedom for a finite element equals the product of number of nodes and the nodal values of the dependent variable required to be computed at every node. Since each finite element is connected at an exterior node with its adjacent element as shown in Figure 4.3(c), the finite element equations are fomulated to maintain the continuity of the dependent variable at each node. However, it is noted that the interelement continuity of the derivatives

of the dependent variable does not necessarily exist. Through this discretization of the domain, a finite element mesh is generated which nearly includes the entire physical domain. In general, triangular elements are known to approximate the domain as well as its boundaries nicely.

4.3.2 LWR-Greenshield's Traffic Flow PDE used in FEM analysis

As introduced earlier in Equation (3.4), the following Traffic Flow PDE is used for numerical simulations using FEM analysis.

$$\frac{\partial \rho}{\partial t} + v_f \frac{\partial \rho}{\partial x} - \frac{2v_f}{\rho_m} \rho \frac{\partial \rho}{\partial x} = 0$$

Since we are only considering the one-dimensional traffic flow problem, the above Equation (3.4) is equivalent to the following Equation (4.11).

$$\rho_t + \left(v_f - \frac{2v_f}{\rho_m} \rho \right) \rho' = 0 \qquad (4.9)$$

This equation is similar to the Navier Stokes Equation as given in Ervin et al. (14). Before introducing the variational formulation for the above equation, let's define a few notations. Considering $\Omega \in \Re$, the $L^2(\Omega)$ norm and the inner product are denoted by $\|.\|$ and $(.,.)$ respectively. For functions $v(x,t)$ defined on entire time interval $(0,T)$, define $\|v\|_{\infty,k} := \sup_{0<t<T} \|v(t,.)\|_k$ and $\|v\|_{m,k} := \left(\int_0^T \|v(t,.)\|_k^m \, dt \right)^{\frac{1}{m}}$. The function space used in FEM analysis is $X := H_0^1(\Omega)$ and the dual space of X is denoted as X', with norm $\|.\|_{-1}$.

A variational formulation of Equation (4.11) can be stated as: Find $\rho \in L^2(0,T;X) \cap$

28

$L^\infty(0, T; L^2(\Omega))$ with $\rho_t \in L^2(0, T; X')$ satisfying

$$
\begin{aligned}
(\rho_t, v) + v_f(\rho', v) - \frac{2v_f}{\rho_m}(\rho \cdot \rho', v) &= 0 \quad , \forall v \in X \\
\rho(x, 0) &= \rho_0(x) \quad , \forall x \in \Omega
\end{aligned}
\tag{4.10}
$$

4.3.3   Finite Element method with Time Relaxation

In this thesis, the diffusion is not being used to solve the hyperbolic traffic flow pde given by Equation (3.4). Due to this, several oscillations exist around the shock solutions. A simple regularization technique was proposed by Adamz , Stoltz and Kleiser in (1) and (2). In this technique, if ρ represents the variable of interest, h represents the characteristic mesh width, and $\delta = O(h)$ a chosen length scale, ρ^* is created to be another variable which represents the part of ρ varying over length scales $< O(\delta)$ i.e. the fluctuating part of ρ. The term $\chi\rho^*$ is then added to the differential equation such that our model in Equation (4.11) is transformed to be,

$$
\rho_t + v_f\rho' - \frac{2v_f}{\rho_m}\rho \cdot \rho' + \chi\rho^* = 0
\tag{4.11}
$$

According to Ervin et al. (14), the term $\chi\rho^*$ drives the unresolved density scales exponentially to zero. The term χ is called as the relaxation coefficient and has the units $\frac{1}{time}$. Now, with the introduction of the new term $\chi\rho^*$, the variational formulation of Equation (4.11) is stated as: Find $\rho \in L^2(0, T; X) \cap L^\infty(0, T; L^2(\Omega))$ with $\rho_t \in L^2(0, T; X')$ satisfying

$$(\rho_t, v) + v_f(\rho', v) - \frac{2v_f}{\rho_m}(\rho \cdot \rho', v) + \chi(\rho - G_N\bar{\rho}, v) \quad = \quad 0 \quad , \forall v \in X$$

$$\rho(x, 0) \quad = \quad \rho_0(x) \quad , \forall x \in \Omega \tag{4.12}$$

In Equation (4.12), $\bar{\rho}$ denotes a spatially averaged function of ρ defined as: $\bar{\rho} := G(\rho)$ satisying

$$-\delta^2 \bar{\rho}'' + \bar{\rho} \quad = \quad \rho \quad , \text{in } \Omega$$

$$\bar{\rho} \quad = \quad 0 \quad , \text{on } \partial\Omega \tag{4.13}$$

where δ represents the filter length scale. According to Ervin et al. (14), the operator G_N in Equation (4.12) represents the Nth van Cittert approximate deconvolution operator defined by

$$G_N\phi := \sum_{n=0}^{N}(I - G)^n\phi, \quad N = 0, 1, 2, \ldots \tag{4.14}$$

For example, the approximate de-convolution operator corresponding to $N = 0, 1, 2$ are $G_0\bar{\rho} = \bar{\rho}$, $G_1\bar{\rho} = 2\bar{\rho} - \bar{\bar{\rho}}$ and $G_2\bar{\rho} = 3\bar{\rho} - 3\bar{\bar{\rho}} + \bar{\bar{\bar{\rho}}}$.

Therefore, for $N = 0$, by substituting $G_0\bar{\rho}$ in Equation (4.12), we get the following system of equations in which the density goes through filtering once:

$$(\rho_t, v) + v_f(\rho', v) - \frac{2v_f}{\rho_m}(\rho \cdot \rho', v) + \chi(\rho - \bar{\rho}, v) \quad = \quad 0 \quad , \forall v \in X$$

$$\rho(x, 0) \quad = \quad \rho_0(x) \quad , \forall x \in \Omega \tag{4.15}$$

where $\bar{\rho}$ is computed through Equation (4.13)

Similarly, for $N = 1$, substituting $G_1\bar{\rho} = 2\bar{\rho} - \bar{\bar{\rho}}$ in Equation (4.12), gives us the following system of equations:

$$
\begin{aligned}
(\rho_t, v) + v_f(\rho', v) - \frac{2v_f}{\rho_m}(\rho \cdot \rho', v) + \chi(\rho - 2\bar{\rho} + \bar{\bar{\rho}}, v) &= 0 \quad , \forall v \in X \\
\rho(x, 0) &= \rho_0(x) \quad , \forall x \in \Omega
\end{aligned}
\tag{4.16}
$$

where $\bar{\rho}$ is first computed through Equation (4.13), which then is used to get $\bar{\bar{\rho}}$ through solving $-\delta^2\, \bar{\bar{\rho}}\,'' + \bar{\bar{\rho}} = \bar{\rho}$. Once $\bar{\bar{\rho}}$ is obtained, the density ρ is computed through Equation (4.17). The same procedure is followed for higher order of deconvolution N, and for $N = 2$, where the system of equations obtained by substituting $G_2\bar{\rho} = 3\bar{\rho} - 3\bar{\bar{\rho}} + \bar{\bar{\bar{\rho}}}$ in Equation (4.12) gives,

$$
\begin{aligned}
(\rho_t, v) + v_f(\rho', v) - \frac{2v_f}{\rho_m}(\rho \cdot \rho', v) + \chi(\rho - 3\bar{\rho} + 3\bar{\bar{\rho}} - \bar{\bar{\bar{\rho}}}, v) &= 0 \quad , \forall v \in X \\
\rho(x, 0) &= \rho_0(x) \quad , \forall x \in \Omega
\end{aligned}
\tag{4.17}
$$

CHAPTER 5

Numerical Simulations

5.1 Introduction

In this chapter, the one-equation Lighthill William and Richards (LWR) model of traffic flow has been studied through two techniques: a) Godunov method and b) Finite element method with time relaxation. For both methods, solutions to several numerical problems found in the research literature are calculated and the comparative results are presented. In all the problems, we compare how godunov solution compares against the finite element solution. For shock problems (Stationary Shock and Shock moving towards right), we investigated how order of relaxation affect the solution, given the same relaxation parameter χ and filter length scale δ.

5.2 Equations

As introduced earlier in (3.3), the following equation is of interest.

$$
\begin{aligned}
\frac{\partial}{\partial t}\rho(t,x) + \frac{\partial}{\partial x}f(\rho) &= 0 \\
f(\rho) &= \rho v(\rho) \\
v(\rho) &= v_f(1 - \frac{\rho}{\rho_m})
\end{aligned}
$$

This equation, when unfolded through substitution of variables, could be written down as follows:

$$\frac{\partial \rho}{\partial t} + \left(v_f - \frac{2v_f}{\rho_m} \rho \right) \frac{\partial \rho}{\partial x} = 0$$

The above equation, given by (3.4) as well, forms the base of the numerical simulations in this chapter. Its variational formulation is given as below. Considering $\Omega \in \Re$

$$
\begin{aligned}
(\rho_t, v) + v_f(\rho', v) - \frac{2v_f}{\rho_m}(\rho \cdot \rho', v) + \chi(\rho - G_N \bar{\rho}, v) &= 0 &, \forall v \in X \\
\rho(x, 0) &= \rho_0(x) &, \forall x \in \Omega
\end{aligned}
$$

For numerical simulations based on finite element method and Backward-Euler temporal discretization with linear extrapolation $\rho^n = 2\rho^{n-1} - \rho^{n-2}$ such that the discretized finite element formualtion for time interval $(0, T]$ could be written as: For $n = 1, 2, \ldots, N_T$, find $\rho_h^n \in X_h$ such that,

$$(\rho_h^n, v) + \Delta t v_f(\rho_h^{n'}, v) - \frac{2v_f}{\rho_m} \Delta t((2\rho_h^{n-1} - \rho_h^{n-2}) \cdot \rho_h^{n'}, v) + \chi \Delta t(\rho_h^n - G_N \bar{\rho}_h^n, v)$$

$$= (\rho_h^{n-1}, v) \forall v \in X_h \quad (5.1)$$

5.3 Accuracy measures

For computation of numerical accuracy, the following measures were used:

1. l^2 *norm of the error*:

The l^2 norm of the error vector e is defined as

$$\|e\| = \sqrt{\sum_{k=1}^{n} |e_k|^2}$$

where e_k represents one term from the error vector and $k = 1, 2, \ldots N$.

2. *Bounded Variation (BV) norm of the error*:

   The bounded variation (bv) norm of the real valued error function defined on

   an interval $[a, b] \subset \Re$ is defined as

   $$V_b^a(e) = \sup_{p \in P} \sum_{i=0}^{n_p - 1} |e(x_{i+1}) - e(x_i)|$$

   where the supremum is taken over the set

   $$\{P = \{x_0, \ldots, x_{nP}\} \,|\, P \ is \ a \ partition \ of \ [a, b]\}$$

3. *Smoothness of Estimated Solution*:

   The inverse of Coefficient of Variation (Wikipedia) can be used for calculating

   the smoothness of the estimated solution. If e represents the error between

   the estimated solution y and it's lag, we can calculate the smoothness of the

   estimated solution $s(e)$ as

   $$s(e) = \frac{|\mu(e)|}{\sigma(e)} = \frac{|\mu(y(2:n-1) - y(1:n-2))|}{\sigma(y(2:n-1) - y(1:n-2))}$$

where n represents the number of data points in the estimated solution.

5.3.1 Comparing the solutions

The accuracy measures defined above are used in comparing different sets of numerical solutions with the exact solutions.

1. *Comparing Godunov and Finite Element Solution*:

   The l^2 norm and the bounded variation (bv) norm of the error defined above are used for numerically comparing the Godunov solution with the FEM solution. In each numerical problem, the l^2 norm and the bounded variation (bv) norm of the error is computed over space and plotted at each time $t \in [0, T]$.

2. *Getting optimal parameters χ and δ for FEM with Time Relaxation*:

   As mentioned above, the Finite Element Method with Time Relaxation method is used for suppressing the oscillations in two problems: a) Stationary Shocks b) Shock moving towards right. Since different combinations of χ and δ give different measures of l^2 norm of the error, bounded variation (bv) norm of the error and smoothness of estimated solution, all the three measures are used to find the best possible χ and δ. The search space consists of the discrete set

   $$\{\chi_{set} \times \delta_{set}\}$$

   where,

   $$\chi_{set} = \{1, 2, 3, \ldots, 100\}, \delta_{set} = \{0.5h, h, 1.5h, 2h, 2.5h, 3h, 3.5h, 4h, 4.5h, 5h\}$$

and h represents the mesh width. Therefore, for the *Stationary Shock* and the *Shock moving towards right* problem, a total of 1000 χ and δ combinations are used to find the best possible χ and δ.

5.4   Common Parameters

This section lists the important parameters that are common to all numerical simulations below.

Parameter Name	Description	Value
a	Beginning point of the road segment	-200
b	Ending point of the road segment	200
l	Length of the road segment	$a - b = 400$ units
T	Final time	5 seconds
M	Number of Nodes	1001
h	FEM Mesh Width	0.3996004
k	Time Step	0.008064516
N	Number of iterations	620
ρ_m	Jam density	0.04
ρ_o	Initial density	0.02
v_f	Free-Flow speed	25

Table 5.1: Common Parameters used in numerical simulations

Apart from the above parameters, the Finite Element method simulations used $P2$ continuous piecewise quadratic basis functions and FreeFEM++ package (6) was used to perform finite element simulations.

5.5   Linear Advection

As introduced in Chapter 3, linear advection refers to the motion of a conserved quantity along a constant vector field. In this problem, since the velocity is constant, the flow is only dependent upon the density. Apart from the common parameters defined above, consider the following parameters:

Parameter Name	Description	Value
c	Advection Velocity	3.0
ρ_l	Left density towards $x = 0^-$ at $t = 0$	0.01
ρ_r	Right density towards $x = 0^+$ at $t = 0$	0.03

Table 5.2: Linear Advection: Parameters used in numerical simulation

Based upon the above parameters ρ_l and ρ_r, the initial density profile we get for this problem is shown in Figure 5.1.
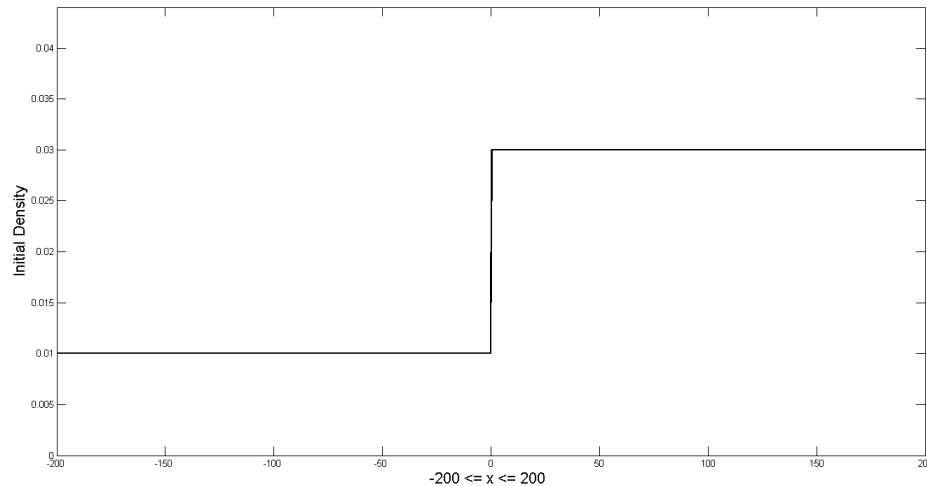

Figure 5.1: Linear Advection: Initial density profile

In the subsequent sections, the numerical techniques introduced in Chapter 4 are used to find the numerical solution to the Linear Advection problem.

5.5.1 Godunov solution

Figure 5.2 provides the Godunov solution of this problem at final time $T = 5$ seconds. Moreover, Figure 5.3 shows the l^2 and the bounded variation (bv) norm of the error for each time $t \in [0, T]$.
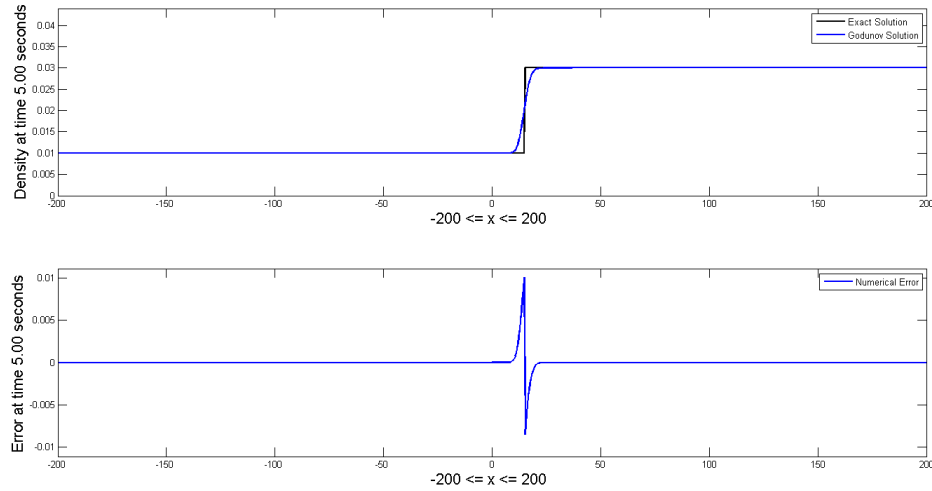

Figure 5.2: Linear Advection: Godunov solution at time $T = 5$ seconds

As observed from the Figures 5.2 and 5.3, the Godunov method simulates this problem well but has a smooth, continuous solution around the discontinuity at time $T = 5$ seconds.

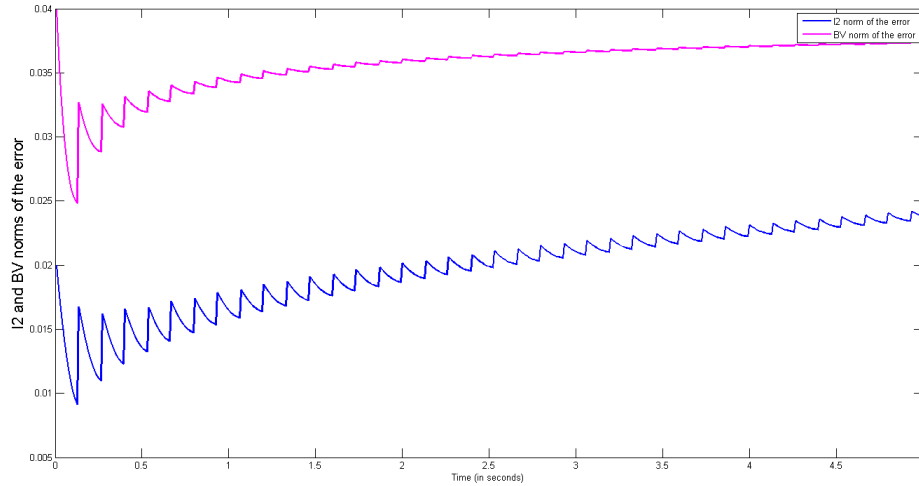Figure 5.3: Linear Advection: l^2 norm and the bounded variation (bv) norm of the error for Godunov solution

5.5.2 FEM solution

Figure 5.4 provides the FEM solution of this problem at final time $T = 5$ seconds.

Moreover, Figure 5.5 shows the l^2 and the bounded variation (bv) norm of the error

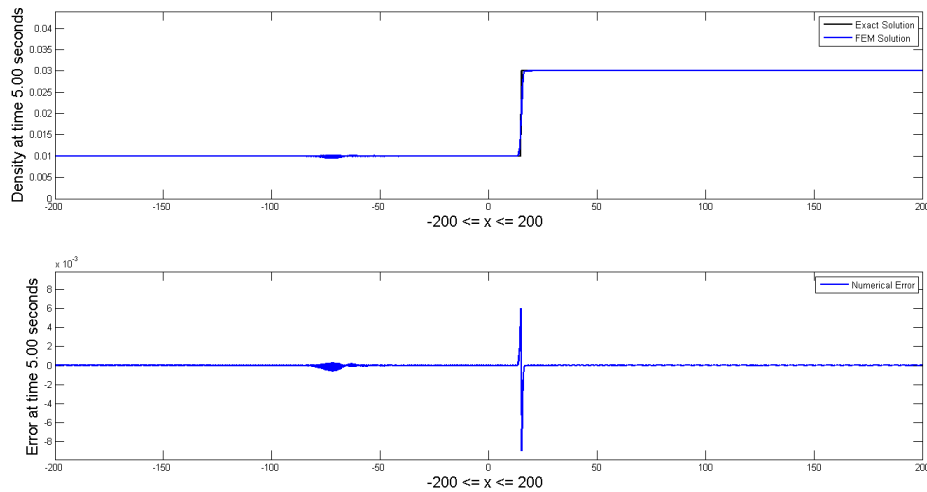for each time $t \in [0, T]$.

Figure 5.4: Linear Advection: FEM solution at time $T = 5$ seconds
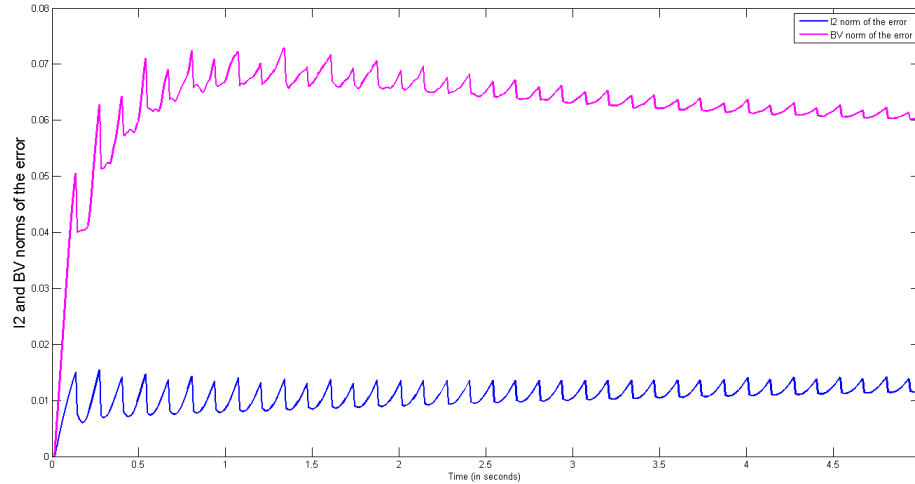
Figure 5.5: Linear Advection: l^2 norm and the bounded variation (bv) norm of the error for FEM solution

As observed from the Figures 5.4 and 5.5, the FEM method simulates this problem well and is able to capture the discontinuity properly.

5.5.3 Comparison of solutions obtained from Godunov method and FEM method

In this section, the numerical results obtained from the Godunov method and FEM method are presented. Figure 5.6 gives an overview of how the Godunov solution compares with the FEM solution at final time $T = 5$ seconds. The l^2 norm and the bounded variation norm of the error obtained from Godunov method and FEM method are also presented in Figure 5.7. The latter figure helps us understand that the FEM method outperforms the Godunov method in terms of the l^2 norm of the error.

Figure 5.6: Linear Advection: Comparison of numerical simulations obtained from Godunov method and FEM method

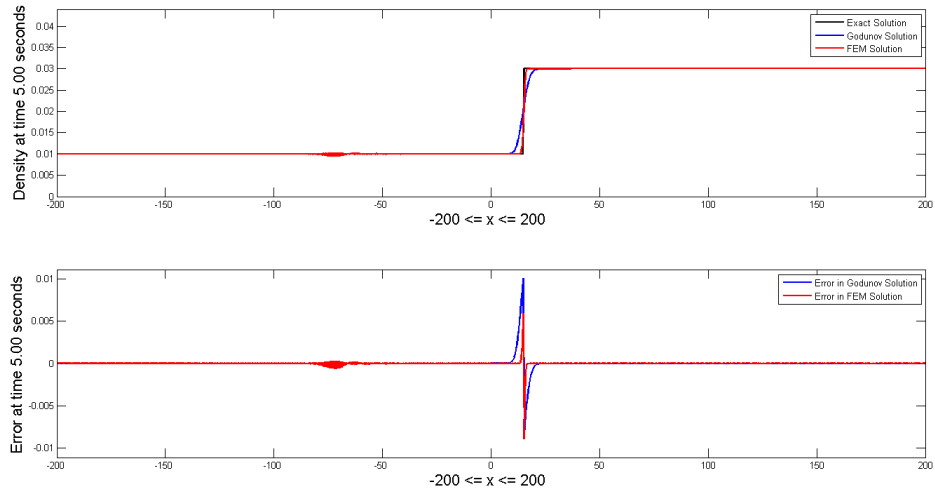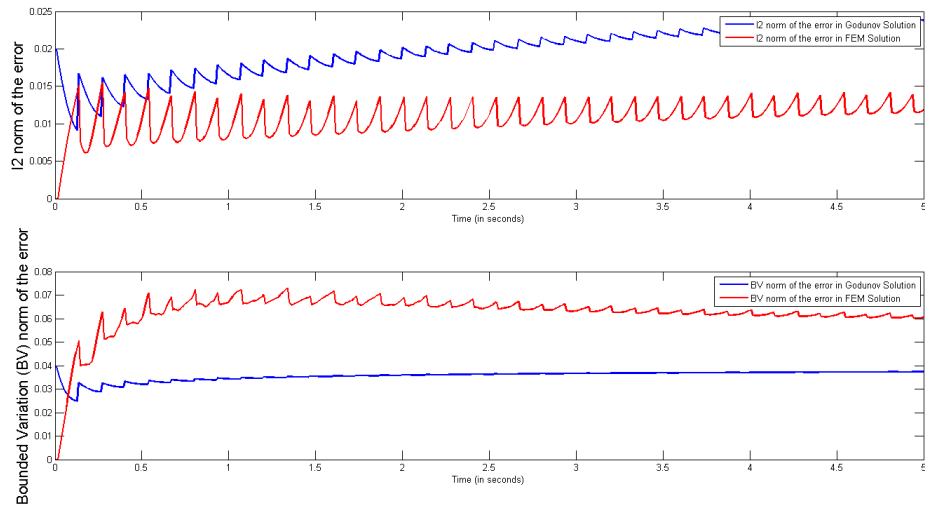

Figure 5.7: Linear Advection: Comparison of l^2 norm and bounded variation (bv) norm of the errors obtained from Godunov method and FEM method

41

5.6 Red Traffic Light turning into Green

As introduced in Chapter 3, when a red traffic light turns into green, a rarefaction wave is formed if $\rho_l > \rho_r$. Apart from the common parameters defined at the beginning of this chapter, consider the following parameters ρ_l and ρ_r:

Parameter Name	Description	Value
ρ_l	Left density towards $x = 0^-$ at $t = 0$	$\rho_m = 0.04$
ρ_r	Right density towards $x = 0^+$ at $t = 0$	0.0

Table 5.3: Red Traffic Light turning into Green: Parameters used in numerical simulation

Based upon the above parameters ρ_l and ρ_r, the initial density profile we get for this problem is shown in Figure 5.8.
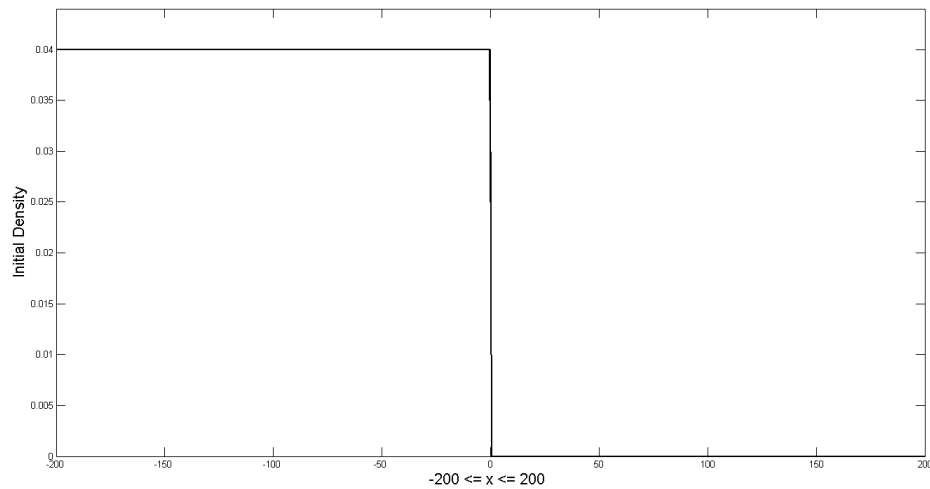
Figure 5.8: Red Traffic Light turning into Green: Initial density profile

In the subsequent sections, the numerical techniques introduced in Chapter 4 are

used to find the numerical solution to this problem.

5.6.1   Godunov solution

Figure 5.9 provides the Godunov solution of this problem at final time $T = 5$ seconds. Moreover, Figure 5.10 shows the l^2 and the bounded variation (bv) norm of the error for each time $t \in [0, T]$.

Figure 5.9: Red Traffic Light turning into Green: Godunov solution at time $T = 5$ seconds

As observed from the Figures 5.9 and 5.10, the Godunov method simulates this problem well.

5.6.2   FEM solution

Figure 5.11 provides the FEM solution of this problem at final time $T = 5$ seconds. Moreover, Figure 5.12 shows the l^2 and the bounded variation (bv) norm of the error

Figure 5.10: Red Traffic Light turning into Green: l^2 norm and the bounded variation (bv) norm of the error for Godunov solution
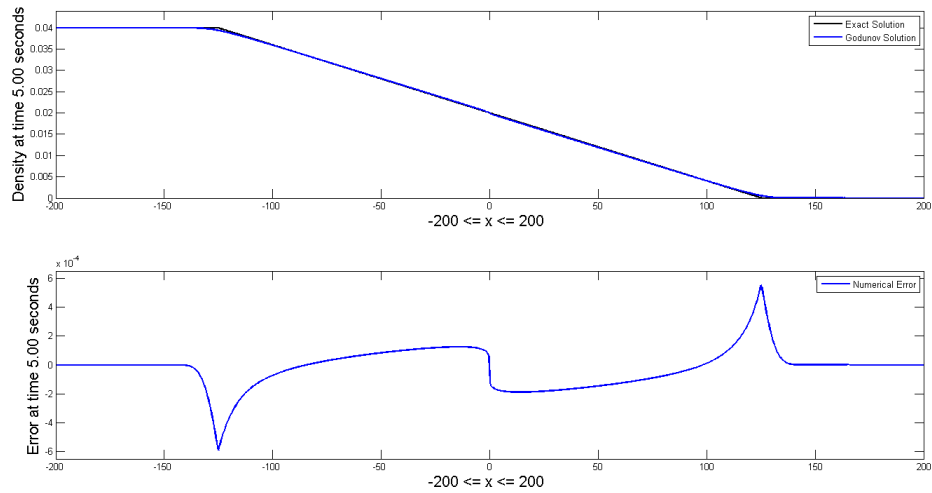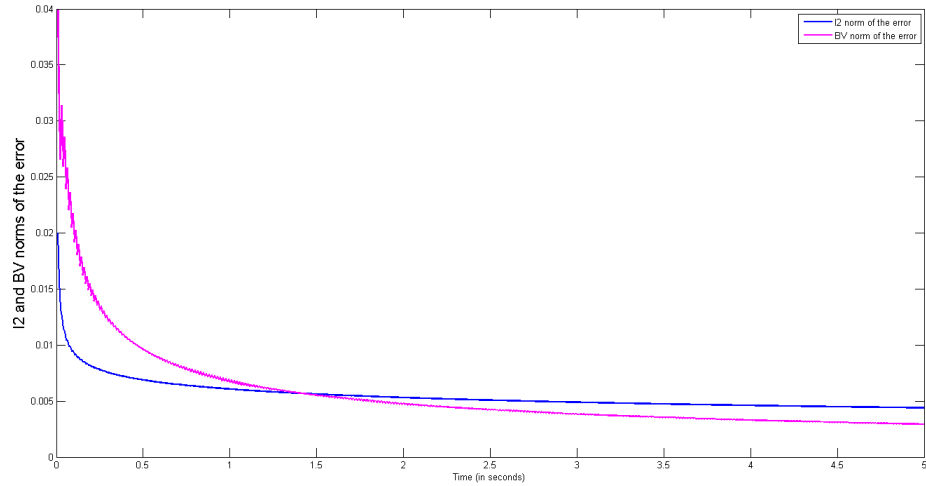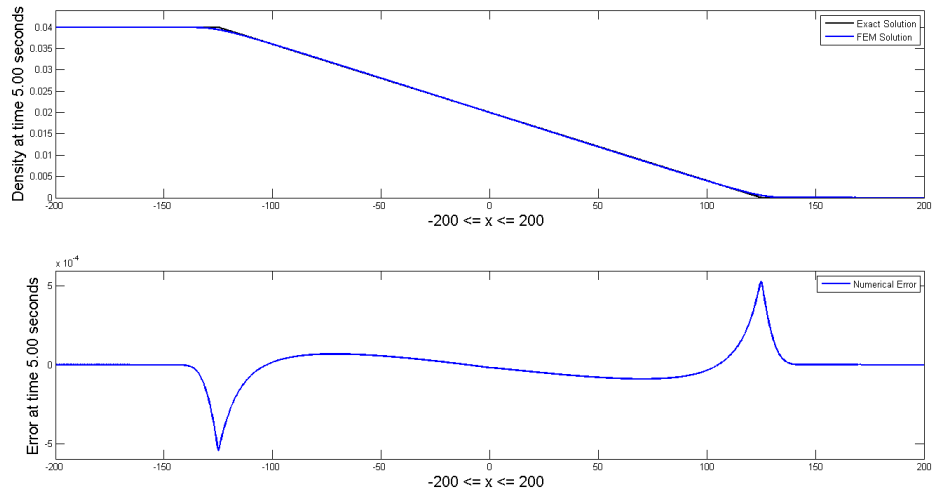
for each time $t \in [0, T]$.

Figure 5.11: Red Traffic Light turning into Green: FEM solution at time $T = 5$ seconds

As observed from the Figures 5.11 and 5.12, the FEM method also simulates this problem well.
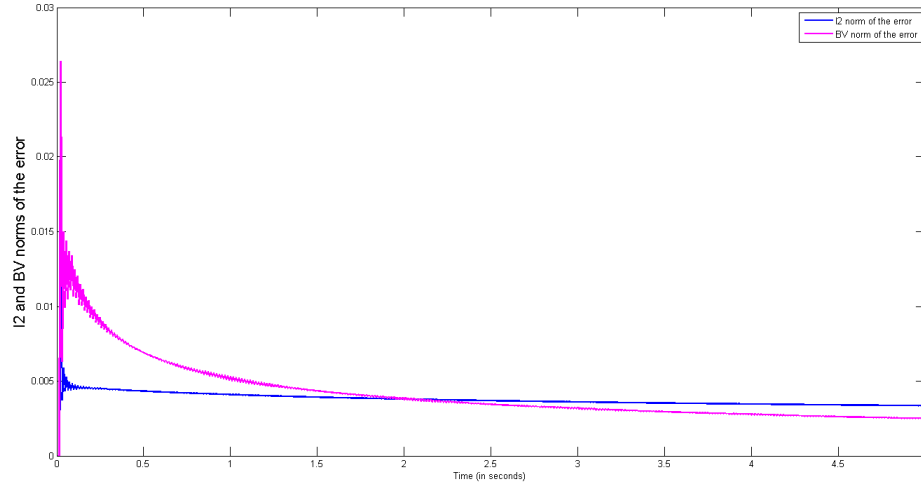
Figure 5.12: Red Traffic Light turning into Green: l^2 norm and the bounded variation (bv) norm of the error for FEM solution

5.6.3 Comparison of solutions obtained from Godunov method and FEM method

In this section, the numerical results obtained from the Godunov method and FEM method are presented. Figure 5.13 gives an overview of how the Godunov solution compares with the FEM solution at final time $T = 5$ seconds. The l^2 norm and the bounded variation norm of the error obtained from Godunov method and FEM method are also presented in Figure 5.14. The latter figure helps us understand that the FEM method outperforms the Godunov method in terms of both, the l^2 norm and the bounded variation norm of the error.

5.7 Stationary Shock

As introduced in Chapter 3, a shock stays stationary if ρ_l and ρ_r are chosen such that the shock velocity remains zero. Apart from the common parameters defined at the beginning of this chapter, consider the following parameters ρ_l and ρ_r:

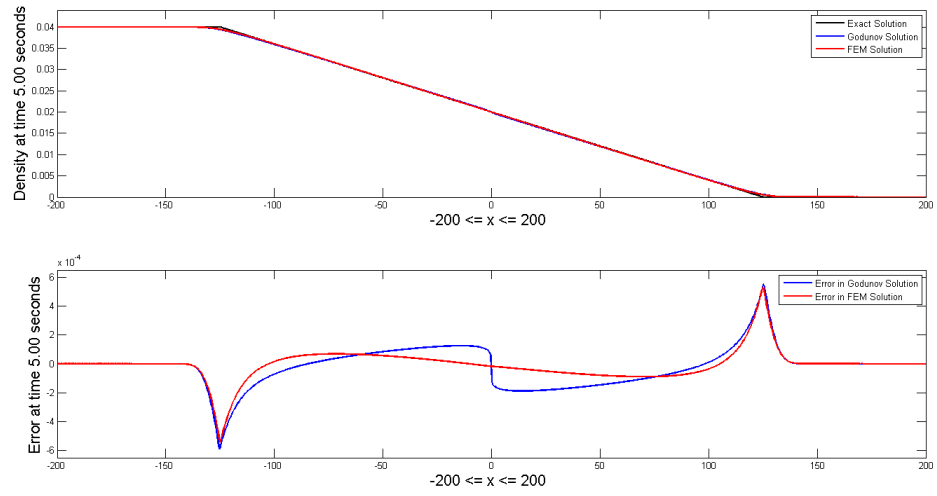Figure 5.13: Red Traffic Light turning into Green: Comparison of numerical simulations obtained from Godunov method and FEM method
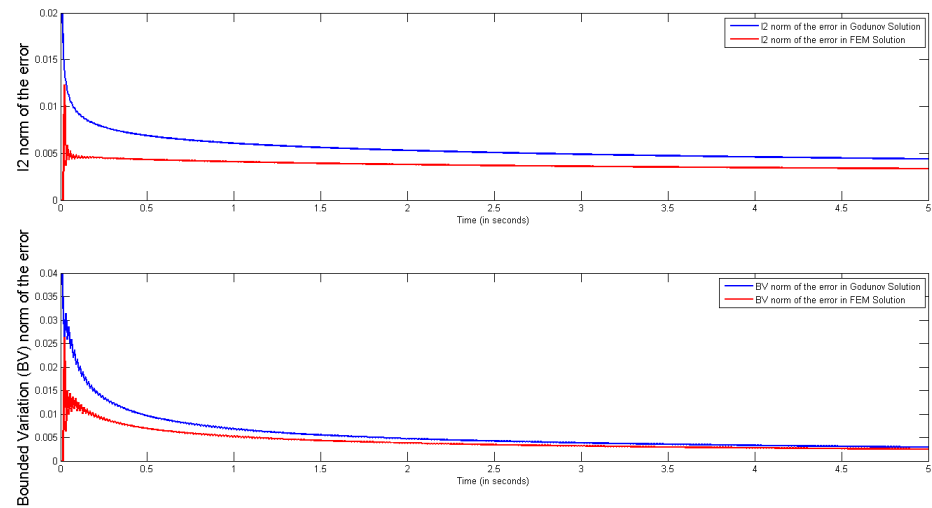
Figure 5.14: Red Traffic Light turning into Green: Comparison of l^2 norm and bounded variation (bv) norm of the errors obtained from Godunov method and FEM method

Parameter Name	Description	Value
ρ_l	Left density towards $x = 0^-$ at $t = 0$	0.01
ρ_r	Right density towards $x = 0^+$ at $t = 0$	0.03

Table 5.4: Stationary Shock: Parameters used in numerical simulation

Based upon the above parameters ρ_l and ρ_r, the initial density profile we get for this problem is shown in Figure 5.15.
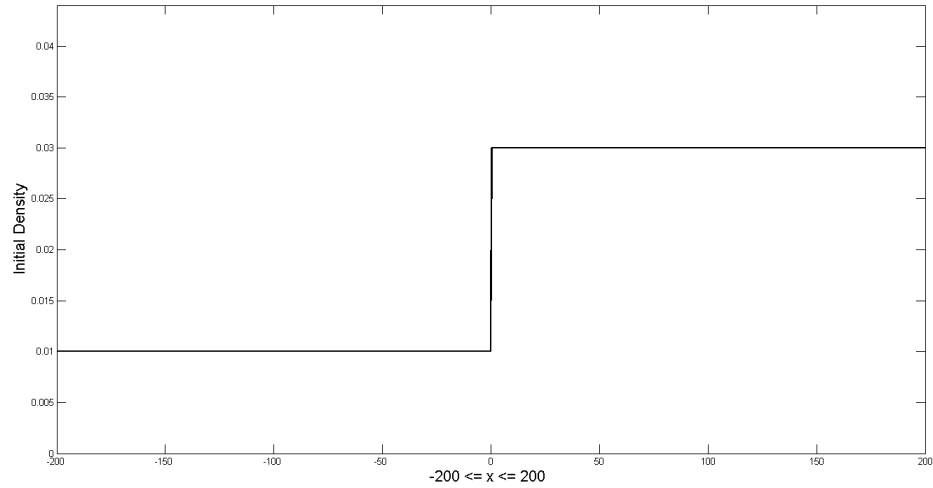
Figure 5.15: Stationary Shock: Initial density profile

For the above ρ_l and ρ_r, the shock speed can be computed from Equation (3.21) as

$$\lambda = \frac{f(\rho_r) - f(\rho_l)}{\rho_r - \rho_l} = \frac{\rho_l * v_f * (1 - \frac{\rho_l}{\rho_m}) - \rho_r * v_f * (1 - \frac{\rho_r}{\rho_m})}{\rho_l - \rho_r}$$

$$\lambda = \frac{0.01 * 25 * (1 - \frac{0.01}{0.04}) - 0.03 * 25 * (1 - \frac{0.03}{0.04})}{0.01 - 0.03} = 0$$

47

Therefore, for the chosen ρ_l and ρ_r, we get shock speed $\lambda = 0$, which causes the shock to remain stationary $\forall\ t > 0$. In the subsequent sections, the numerical techniques introduced in Chapter 4 are used to find the numerical solution to this problem.

5.7.1   Godunov solution

Figure 5.16 provides the Godunov solution of this problem at final time $T = 5$ seconds. Moreover, Figure 5.17 shows the l^2 and the bounded variation (bv) norm of the error for each time $t \in [0, T]$.
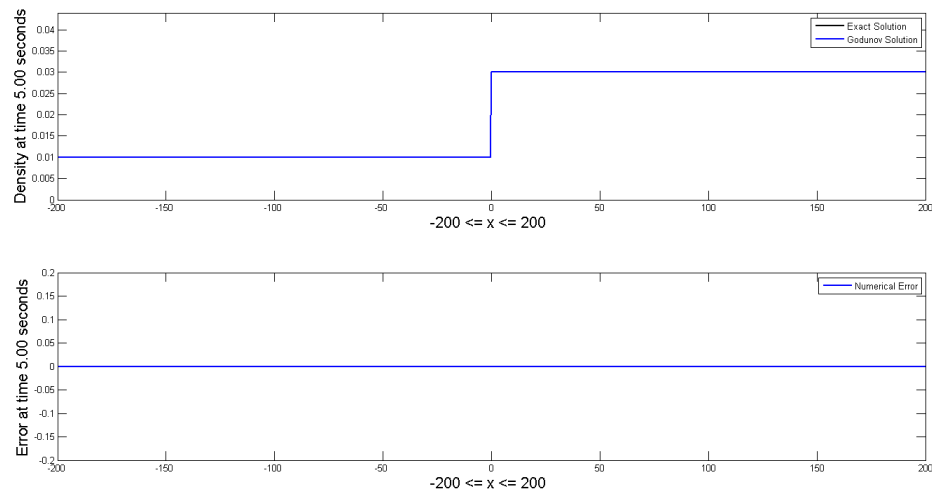

Figure 5.16: Stationary Shock: Godunov solution at time $T = 5$ seconds

As observed from the Figures 5.16 and 5.17, it seems that the Godunov method simulates the stationary shock extremely well. This is because the Godunov solution is based upon the flow at the left and right junctions of a segment, but since the shock
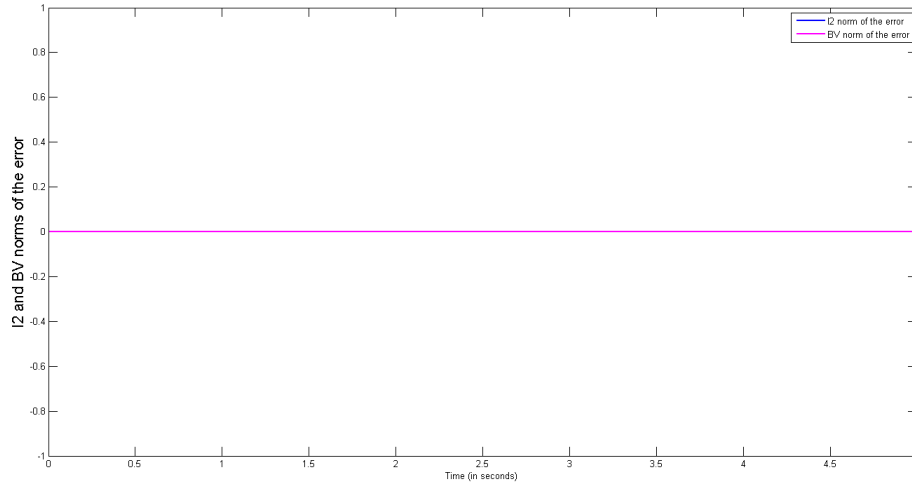
Figure 5.17: Stationary Shock: l^2 norm and the bounded variation (bv) norm of the error for Godunov solution

velocity is 0, the flow is 0. Hence, the solution keeps it's initial profile $\forall t > 0$.

5.7.2 FEM solution without time relaxation

In Equation (4.12), the relaxation parameter χ can be set to 0 to yield a finite element variational problem without any relaxation. Figures 5.18 and 5.19 provide the FEM solution at the final time $T = 5$ seconds and the l^2 and the bounded variation (bv) norm of the error for each time $t \in [0, T]$ respectively.

As can be observed in the Figures 5.18 and 5.19, the finite element method is not able to numerically simulate the stationary shock and gets tremendous amounts of oscillations.

5.7.3 FEM solution with time relaxation

As introduced in Chapter 4, the term $\chi \rho^*$ can be added to the finite element variation formulation, which helps to drive the unresolved density scales exponentially
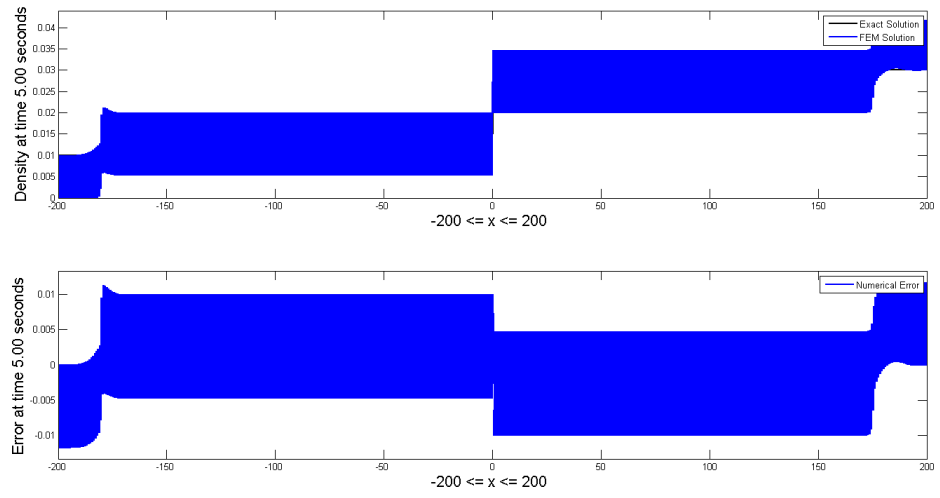
49

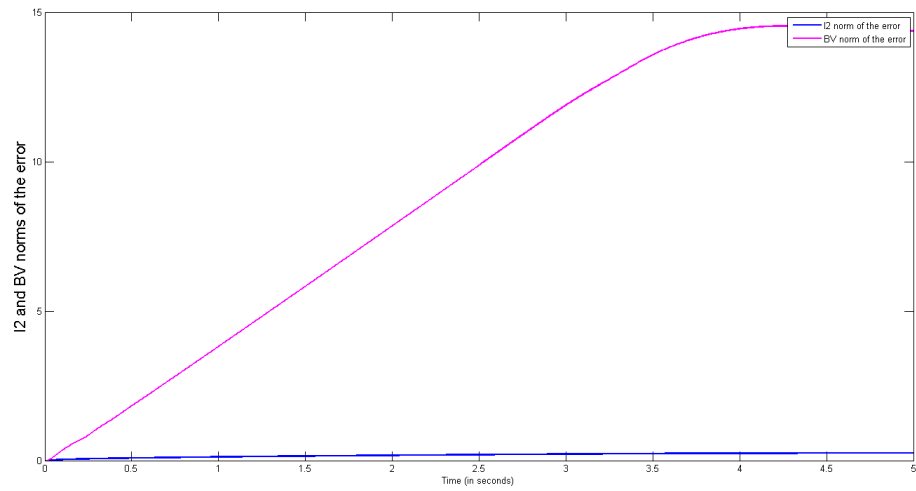Figure 5.18: Stationary Shock: FEM solution without any time relaxation

Figure 5.19: Stationary Shock: l^2 norm and bounded variation (bv) norm of the error for FEM solution without any time relaxation

to zero. The finite element variational formulation with time relaxation was given in the beginning of this chapter and also, in Chapter 4.

However, the usage of time relaxation in finite element method requires choosing the relaxation parameter χ and filter length scale δ. Based upon the process described earlier in this chapter, numerical computations were done to get the optimal χ and δ over 1000 such combinations.

For all such combinations, l^2 norm of the error, bounded variation (bv) norm of the error and the smoothness of the estimated solution were calculated by performing time relaxation twice, whose variational formulation is given in Chapter 4. Following steps were taken to choose the optimal χ and δ.

1. In order to reduce the search space, only those candidates of $\chi - \delta$ combinations were selected for which $min(l^2) < l^2 < 1.3 * min(l^2)$.

2. From amongst the above candidates, that $\chi - \delta$ combination was chosen which gave the minimal bounded variation (bv) norm of the error and the maximum smoothness of the estimated solution.

The results are presented in Figure 5.20.

As observed in Figure 5.20, $\chi = 100$ and $\delta = 0.5h$ resulted in minimal l^2 norm of the error. Additionally, it had the minimal bounded variation (bv) norm of the error and led to maximum smoothness of the estimated solution. With the chosen parameters $\chi = 100$ and $\delta = 0.5h$ and time relaxation with $N = 1$ in finite element method, the results obtained are shown in Figures 5.21 and 5.22 . Figure 5.21 provides the FEM solution for Time Relaxation with $N = 1$ at the final time $T = 5$ seconds.
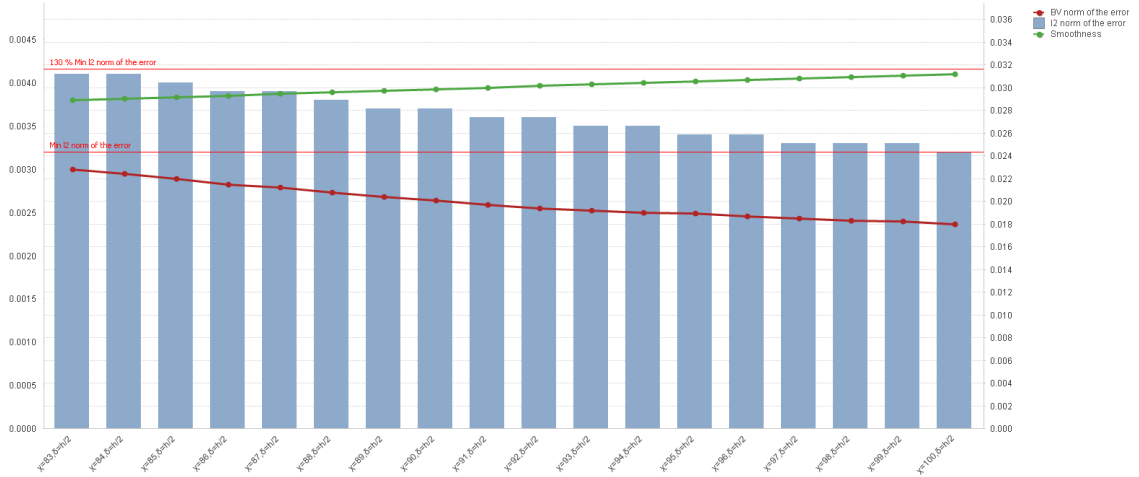
Figure 5.20: Stationary Shock: Usage of l^2 norm of the error, bounded variation (bv) norm of the error and Smoothness of Estimated Solution to find the optimal $\chi - \delta$ combination.

Additionally, Figure 5.22 provides the l^2 norm and the bounded variation (bv) norm of the error for each time $t \in [0, T]$ respectively.
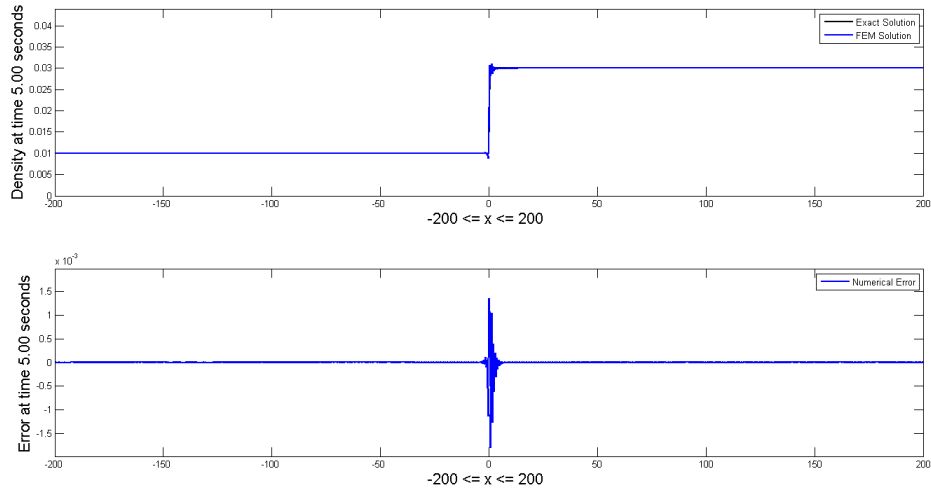
Figure 5.21: Stationary Shock: FEM solution for Time Relaxation with $N = 1$

For the chosen parameter: $\chi = 100$ and $\delta = 0.5h$, a comparison was also performed on how different orders deconvolution of time relaxation affects the numerical

52
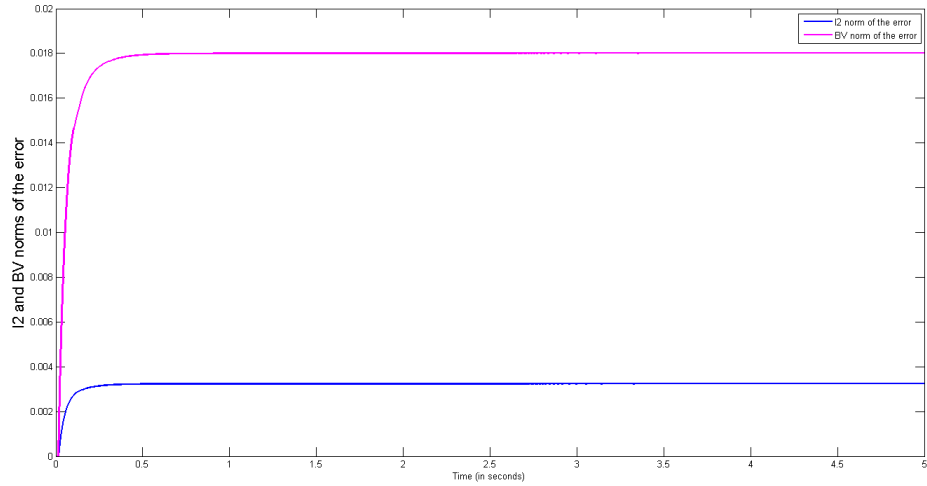
Figure 5.22: Stationary Shock: l^2 norm and bounded variation (bv) norm of the error for FEM solution with Time Relaxation and $N = 1$

simulations of the stationary shock problem. This comparison is provided in Figures 5.23 and 5.24.

Figure 5.23: Stationary Shock: FEM solutions for different orders of time relaxation schemes where $\chi = 100$ and $\delta = 0.5h$

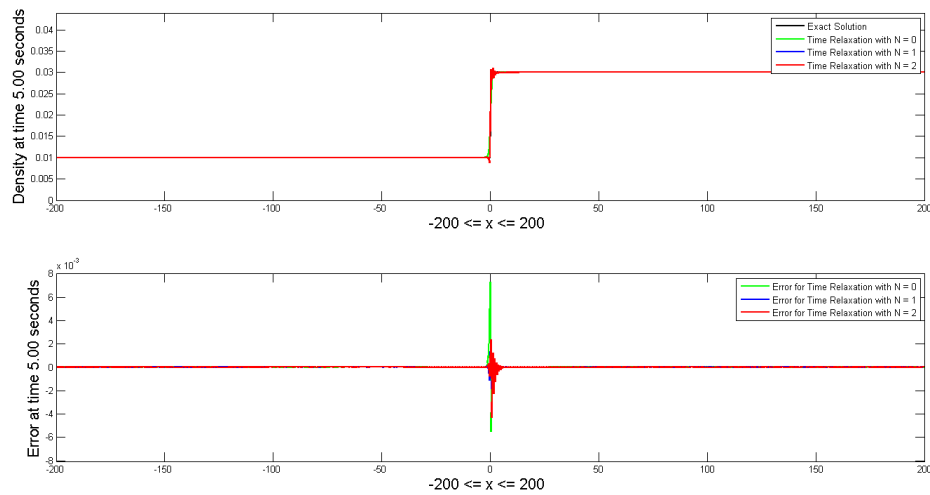From Figure 5.24, it can be observed that the performance of FEM time relaxation
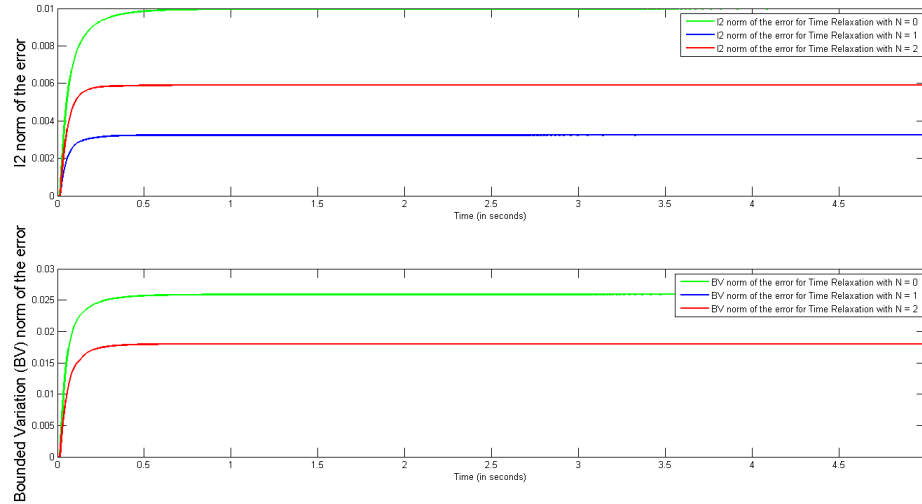
Figure 5.24: Stationary Shock: l^2 norm and bounded variation (bv) norm of the error for different orders of time relaxation schemes where $\chi = 100$ and $\delta = 0.5h$

twice is much better than the time relaxation once and thrice. Hence, performing time relaxation twice on the finite elements should suffice to get an acceptable solution of stationary shock problem without much oscillations.

5.7.4 Comparison of solutions obtained from Godunov method and FEM time relaxation method

In this section, the numerical results obtained from the Godunov method and FEM method with time relaxation and $N = 1$ ($\chi = 100$ and $\delta = 0.5h$) are presented. Figure 5.25 gives an overview of how the Godunov solution compares with the FEM solution at final time $T = 5$ seconds. The l^2 norm and the bounded variation norm of the error obtained from Godunov method and FEM method presented in Figure 5.26, provide a better understanding of the comparative performance of the two solutions for this numerical problem. From the latter figure, it can be observed that the Godunov

solution outperformed the FEM solution.
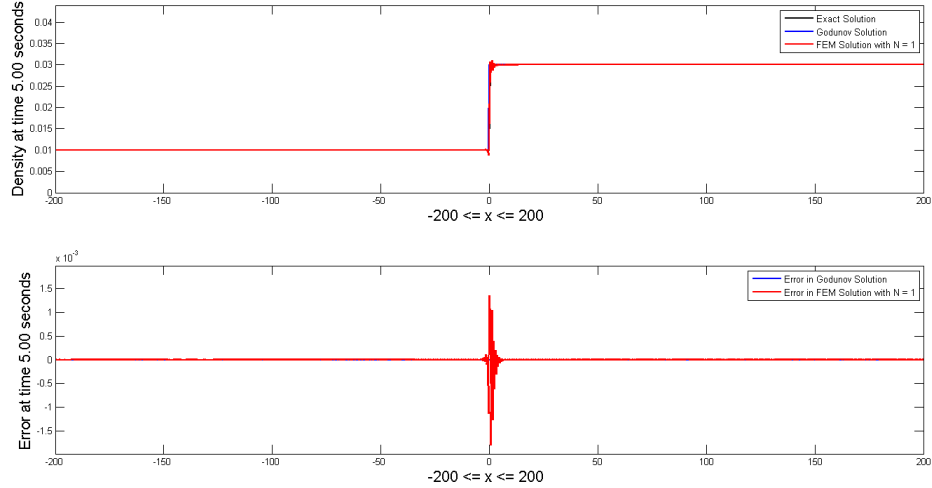
Figure 5.25: Stationary Shock: Comparison of numerical simulations obtained from Godunov method and FEM method for Time Relaxation with $N = 1$

5.8 Shock moving towards right

As introduced in Chapter 3, a shock moves towards right if ρ_l and ρ_r are chosen such that the shock velocity becomes positive. Consider the following parameters ρ_l and ρ_r:

Parameter Name	Description	Value
ρ_l	Left density towards $x = 0^-$ at $t = 0$	0.01
ρ_r	Right density towards $x = 0^+$ at $t = 0$	0.025

Table 5.5: Parameters used in numerical simulation of a shock moving towards right

Based upon the above parameters ρ_l and ρ_r, the initial density profile we get for
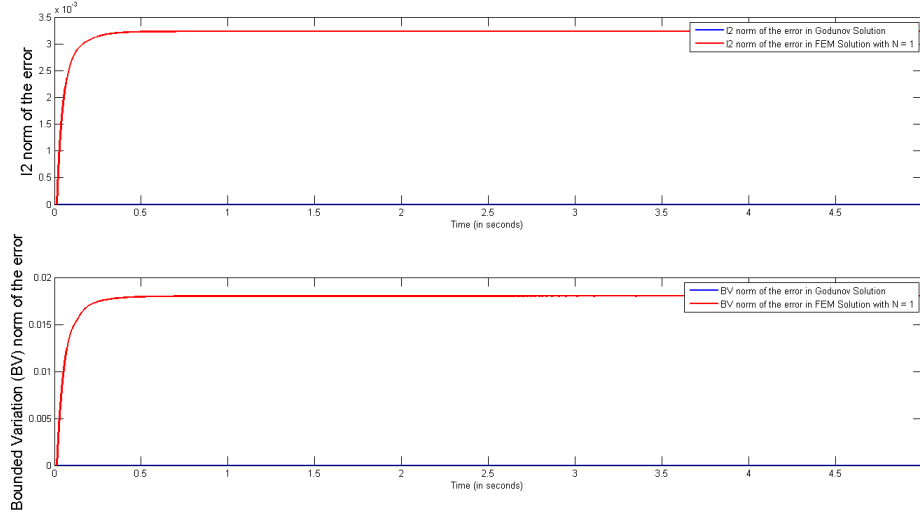
Figure 5.26: Stationary Shock: Comparison of l^2 norm and bounded variation (bv) norm of the errors obtained from Godunov method and FEM method for Time Relaxation with $N = 1$

this problem is shown in Figure 5.27.

For the above ρ_l and ρ_r, the shock speed can be computed from Equation (3.21) as

$$\lambda = \frac{f(\rho_r) - f(\rho_l)}{\rho_r - \rho_l} = \frac{\rho_l * v_f * \left(1 - \frac{\rho_l}{\rho_m}\right) - \rho_r * v_f * \left(1 - \frac{\rho_r}{\rho_m}\right)}{\rho_l - \rho_r}$$

$$\lambda = \frac{0.01 * 25 * \left(1 - \frac{0.01}{0.04}\right) - 0.025 * 25 * \left(1 - \frac{0.025}{0.04}\right)}{0.01 - 0.025} = 3.125$$

Therefore, for the chosen ρ_l and ρ_r, we get shock speed $\lambda > 0$, which causes the shock to move towards right. In the subsequent sections, the numerical techniques introduced in Chapter 4 are used to find the numerical solution to this problem.

56

Figure 5.27: Shock moving towards right: Initial density profile

5.8.1 Godunov solution

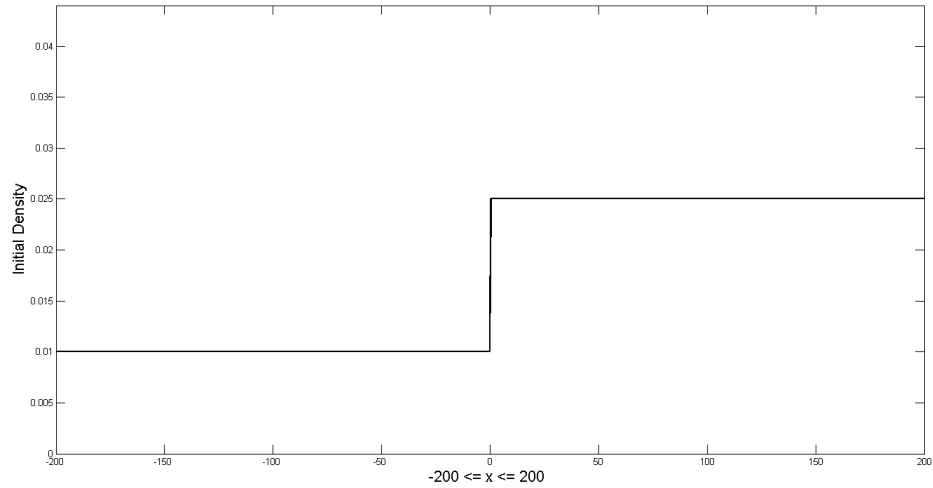Figure 5.28 provides the Godunov solution of this problem at final time $T = 5$ seconds. Moreover, Figure 5.29 shows the l^2 and the bounded variation (bv) norm of the error for each time $t \in [0, T]$.

Figure 5.28: Shock moving towards right: Godunov solution at time $T = 5$ seconds

Figure 5.29: Shock moving towards right: l^2 norm and the bounded variation (bv) norm of the error for Godunov solution

5.8.2 FEM solution without time relaxation

In Equation (4.12), the relaxation parameter χ can be set to 0 to yield a finite element variational problem without any relaxation. Figures 5.30 and 5.31 provide the FEM solution at the final time $T = 5$ seconds and the l^2 and the bounded variation (bv) norm of the error for each time $t \in [0, T]$ respectively.
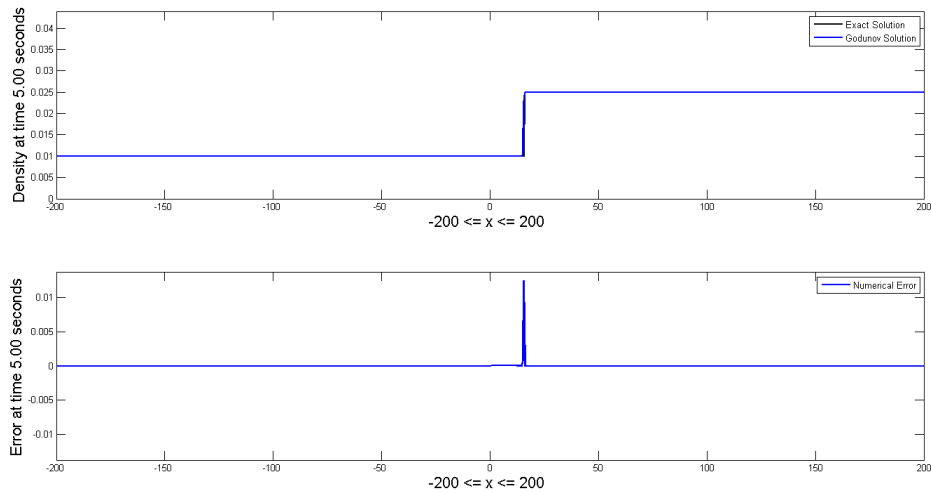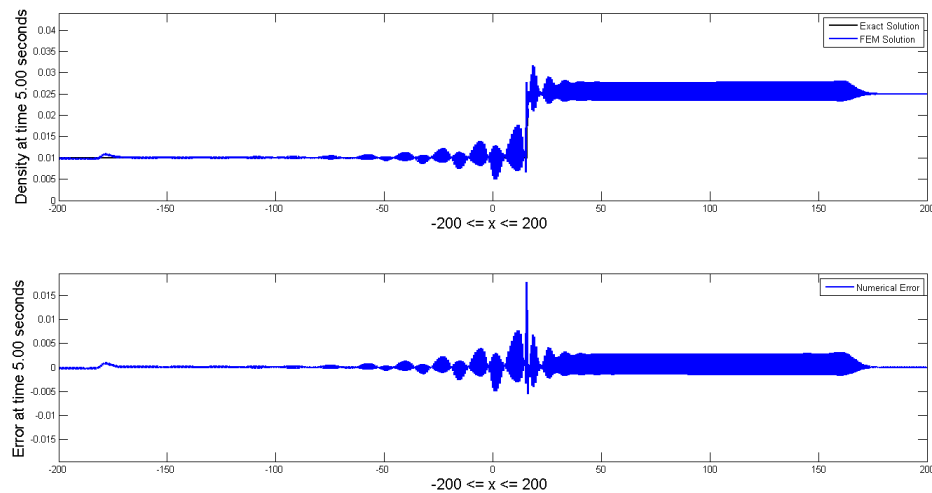

Figure 5.30: Shock moving towards right: FEM solution without any time relaxation
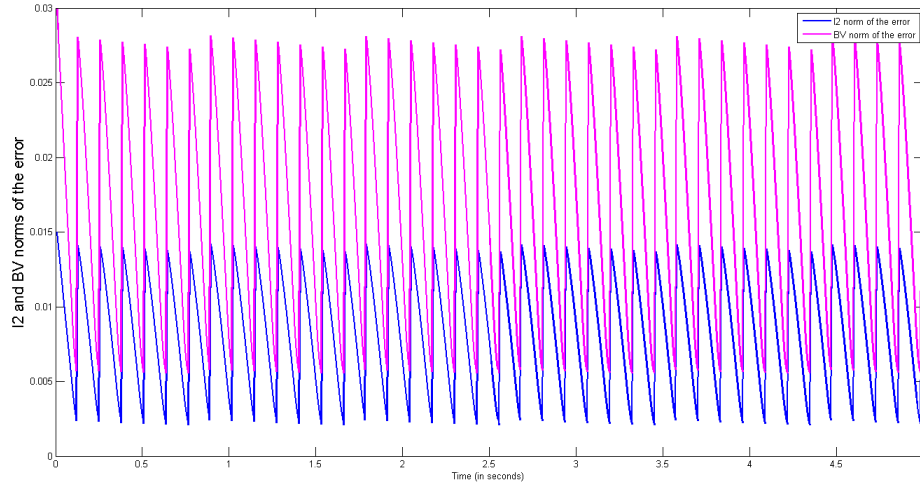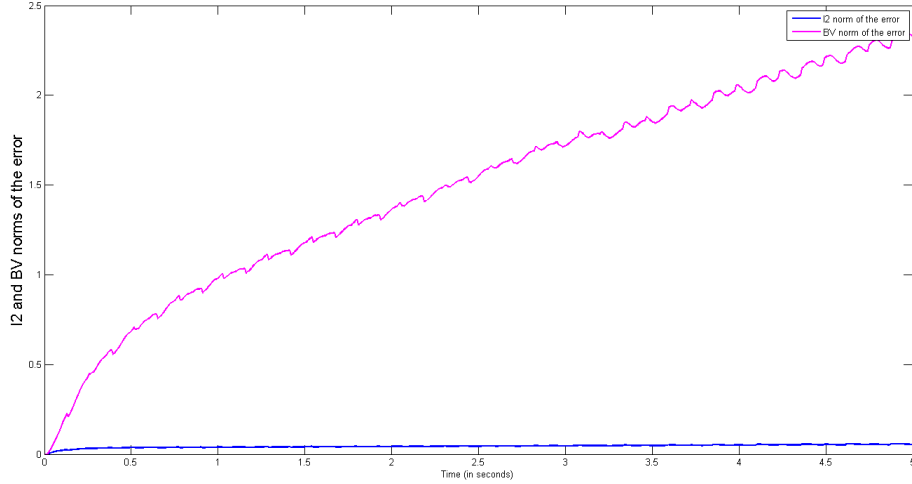
Figure 5.31: Shock moving towards right: l^2 norm and bounded variation (bv) norm of the error for FEM solution without any time relaxation

As can be observed in the Figures 5.30 and 5.31, the finite element method is not able to numerically simulate the moving shock and gets tremendous amounts of oscillations.

5.8.3   FEM solution with time relaxation

As introduced in Chapter 4, the term $\chi \rho^*$ can be added to the finite element variation formulation, which helps to drive the unresolved density scales exponentially to zero. The finite element variational formulation with time relaxation was given in the beginning of this chapter and also, in Chapter 4.

However, the usage of time relaxation in finite element method requires choosing the relaxation parameter χ and filter length scale δ. Based upon the process described earlier in this chapter, numerical computations were done to get the optimal χ and δ over 1000 such combinations.

For all such combinations, l^2 error, bounded variation and the smoothness of the estimated solution were calculated by performing time relaxation twice, whose variational formulation is given in Chapter 4. Following steps were taken to choose the optimal χ and δ.

1. In order to reduce the search space, only those candidates of $\chi - \delta$ combinations were selected for which $min(l^2) < l^2 < 1.09 * min(l^2)$.

2. From amongst the above candidates, that $\chi - \delta$ combination was chosen which gave the minimal bounded variation (bv) norm of the error and the maximum smoothness of the estimated solution.

The results are presented in Figure 5.32.

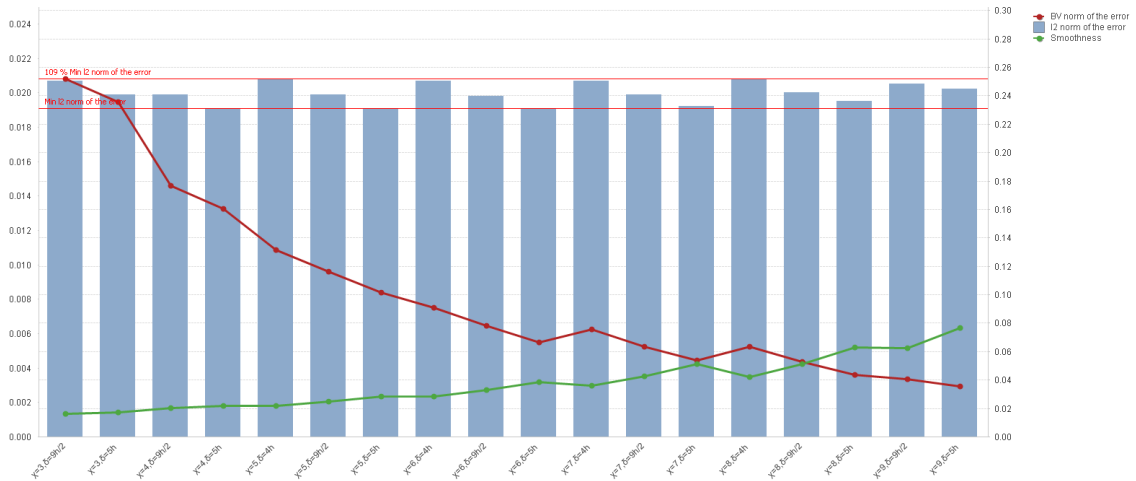Figure 5.32: Shock moving towards right: Usage of l^2 norm of the error, Bounded Variation (bv) norm of the error and Smoothness of Estimated Solution to find the optimal $\chi - \delta$ combination.

As observed in Figure 5.32, $\chi = 9$ and $\delta = 5h$ resulted in l^2 norm of the error

60

to be within 109% of the minimum l^2 norm of the error. Additionally, it had the minimal bounded variation (bv) norm of the error and led to maximum smoothness of the estimated solution. With the chosen parameters $\chi = 9$ and $\delta = 5h$ and twice relaxation in finite element method, the results obtained are shown in Figures 5.33 and 5.34 . Figure 5.33 provides the FEM solution for Time Relaxation with $N = 1$ at the final time $T = 5$ seconds. Additionally, Figure 5.34 provides the l^2 norm and the bounded variation (bv) norm of the error for each time $t \in [0, T]$ respectively.
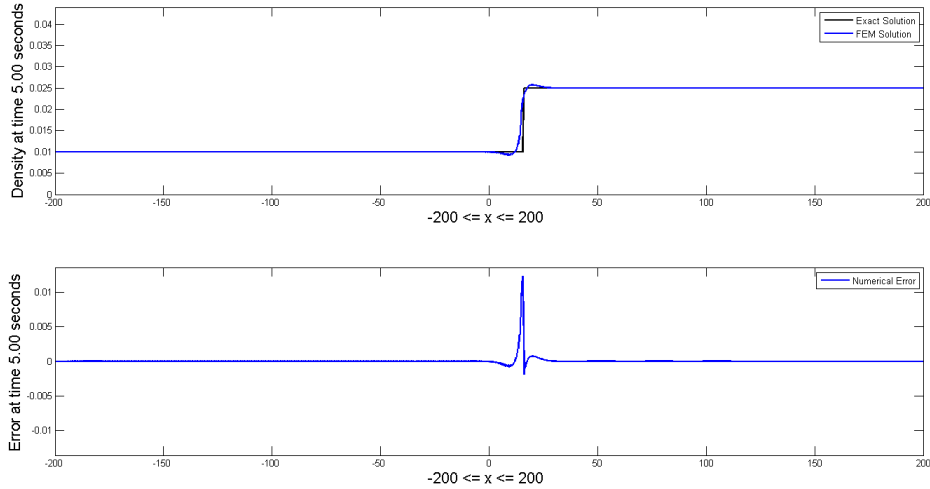
Figure 5.33: Shock moving towards right: FEM solution for Time Relaxation with $N = 1$

For the chosen parameter: $\chi = 9$ and $\delta = 5h$, a comparison was also performed on how different orders of time relaxation affects the numerical simulations. This comparison is provided in Figures 5.35 and 5.36.

From Figure 5.36, it can be observed that the performance of FEM time relaxation with $N = 2$ and $N = 1$ is better than $N = 0$ case. However, the performance of FEM

Figure 5.34: Shock moving towards right: l^2 norm and bounded variation (bv) norm of the error in FEM solution for Time Relaxation with $N = 1$
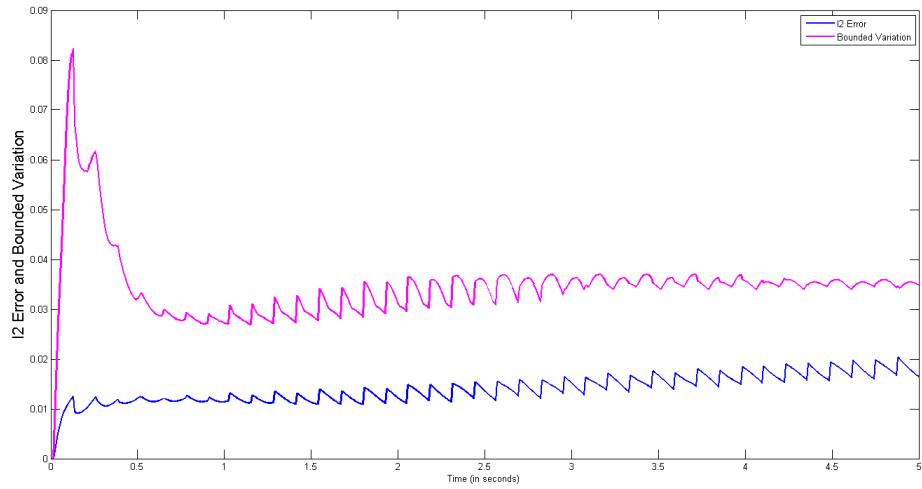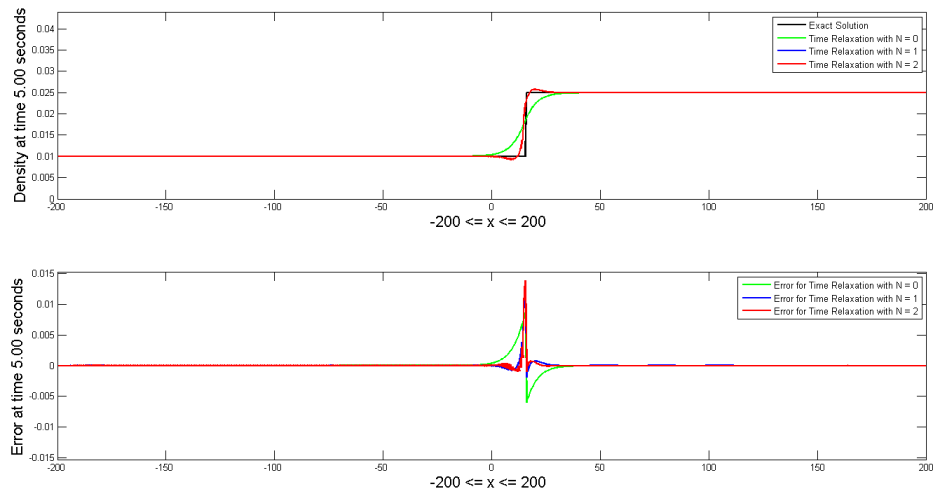

Figure 5.35: Shock moving towards right: FEM solutions for different orders of time relaxation schemes where $\chi = 9$ and $\delta = 5h$
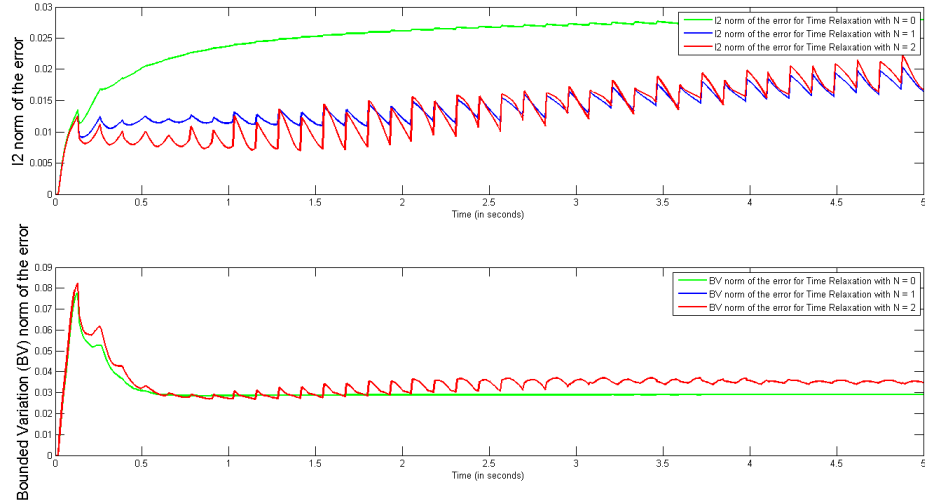
Figure 5.36: Shock moving towards right: l^2 norm and bounded variation (BV) norm of the errors for different orders of time relaxation schemes where $\chi = 9$ and $\delta = 5h$

time relaxation $N = 1$ and $N = 2$ is comparable for the chosen time relaxation parameters. Hence, performing time relaxation with $N = 1$ on the finite elements should suffice to get an acceptable solution without much oscillations.

5.8.4 Comparison of solutions obtained from Godunov method and FEM time relaxation method

In this section, the numerical results obtained from the Godunov method and FEM method for Time Relaxation with $N = 1$ ($\chi = 9$ and $\delta = 5h$) are presented. Figure 5.37 gives an overview of how the Godunov solution compares with the FEM solution at final time $T = 5$ seconds. The l^2 norm and the bounded variation norm of the error obtained from Godunov method and FEM method presented in Figure 5.38, provide a better understanding of the comparative performance of the two solution for this numerical problem. From the latter figure, it can be observed that the Godunov

solution outperformed the FEM solution because although the FEM solution captured the movement of the shock and did not give any oscillations, the FEM solution was smoothed around the discontinuity. However, the Godunov solution not only captured the movement without much oscillations, but also gave the expected shape of the discontinous curve.

Figure 5.37: Shock moving towards right: Comparison of numerical simulations obtained from Godunov method and FEM method for Time Relaxation with $N = 1$
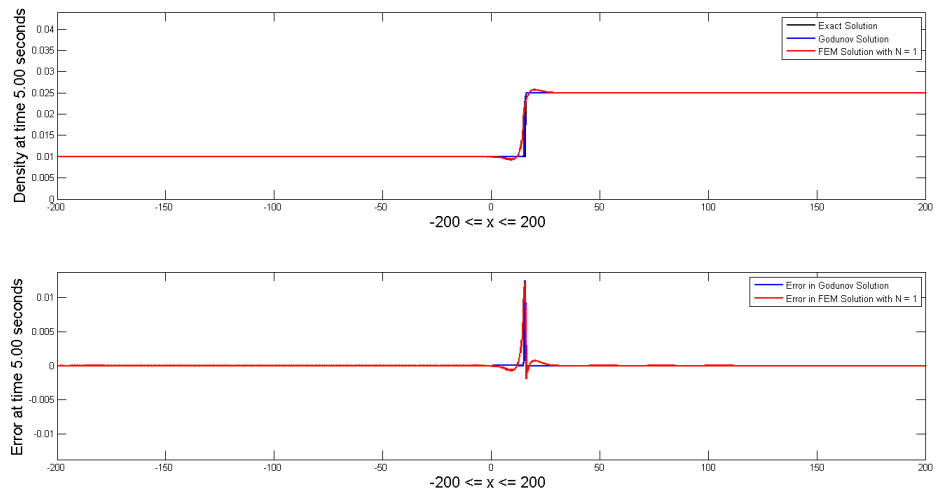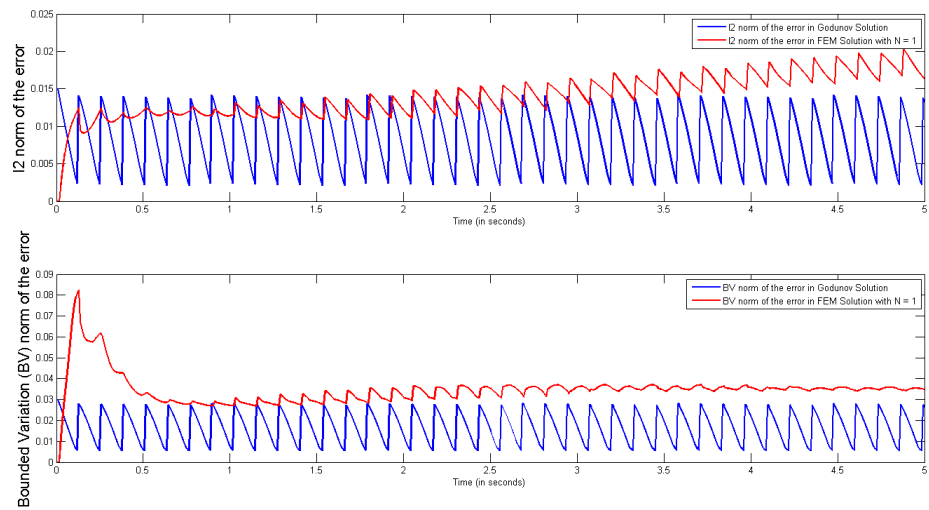
Figure 5.38: Shock moving towards right: Comparison of l^2 norm and bounded variation (bv) norm of the errors obtained from Godunov method and FEM method for Time Relaxation with $N = 1$

CHAPTER 6

Conclusion

6.1   Summary

This thesis applied numerical methods popular in fluid research into traffic flow problems. Several numerical simulations for the LWR and Greenshield's model were presented using both, the Godunov and the Finite Element method. The application of time relaxation within finite elements allowed finite element simulations to get rid of the diffusion term and suppress oscillations just by fine tuning the time relaxation parameters χ and δ.

It was observed that:

1. Finite Element Method outperformed Godunov method in two problems:

   - Linear Advection

   - Red Traffic Light turning into Green

2. Godunov method outperformed Finite Element Time Relaxation method in two problems:

   - Stationary Shocks

   - Shock moving towards right

3. In presence of shocks, the Finite Element Method performs bad and has lots of oscillations, if no time relaxation is added. However, addition of time relaxation suppresses oscillations to a great extent.

4. Increasing the order of time relaxation does not necessarily mean that the solution will become more smooth and will have better properties. As observed, doing time relaxation with $N = 1$ outperformed time relaxation with $N = 0$ and $N = 2$. This was clearly observed in Stationary Shocks, however, the performance of time relaxation with $N = 1$ was close to time relaxation with $N = 2$ for Shock moving towards Right.

5. l^2 norm of the error, bounded variation norm of the error and the smoothness of the estimated solution proved to be extremely helpful measures in selecting the right candidates for optimal parameters χ and δ.

6.2 Future Work

This section presents the following areas where the thesis can be extended for further research.

1. Currently, the numerical simulations were computed using the LWR and Greenshield's model. However, Kachroo (9) presents other models for the velocity density relationship where the numerical simulations can be performed using the Godunov and Finite Element Methods. A few of those models are shown below:

   - Greenberg model: $v(\rho) = v_f \ln \left(\dfrac{\rho_m}{\rho} \right)$
   - Underwood model: $v(\rho) = v_f \exp \left(-\dfrac{\rho}{\rho_m} \right)$
   - Northwestern University model: $v(\rho) = v_f exp \left(-0.5(\dfrac{\rho}{\rho_m})^2 \right)$

67

2. In this thesis, numerical simulations were performed for four benchmark problems. The simulations can be performed for other problems as well such as: a shock moving towards left.

3. The thesis can be further extended by performing higher order discretization in time with Crank-Nicolson schemes, theta schemes etc. Please see Volker (8) for more details.

4. Last but not the least, a non linear time relaxation can be performed that can perform better reduction in oscillations more efficiently. Please see Layton (10) for more details.

BIBLIOGRAPHY

[1] Adams, N. and Stolz, S. (2001). Deconvolution methods for subgrid-scale approximation in large eddy simulation. *Modern Simulation Strategies for Turbulent Flow*, pages 21–41.

[2] Adams, N. and Stolz, S. (2002). A subgrid-scale deconvolution approach for shock capturing. *Journal of Computational Physics*, 178(2):391–426.

[3] Bellomo, N. and Delitala, M. (2002). On the mathematical theory of vehicular traffic. *Fluid Dynamic and Kinetic Modeling*, I.

[4] Gerlough, D. L. and Huber, M. J. (1975). *Traffic flow theory: a monograph*, volume 165. Transportation Research Board, National Research Council Washington, DC.

[5] Haberman, R. (1998). *Mathematical Models: mechanical vibrations, population dynamics and traffic flow*. Society for Industrial and Applied Mathematics.

[6] Hecht, F. (2012). New development in freefem++. *J. Numer. Math.*, 20(3-4):251–265.

[7] Hutton, D. V. (2004). *Fundamentals of Finite Element Analysis*. McGraw-Hill.

[8] John, V. (2004). *Large eddy simulation of turbulent incompressible flows: analytical and numerical results for a class of LES models*, volume 34. Springer.

[9] Kachroo, P. (2009). *Pedestrian Dynamics: mathematical theory and evaculation control*. CRC Press.

[10] Layton, W. and Neda, M. (2007). Truncation of scales by time relaxation. *Journal of Mathematical Analysis and Applications*, 325(2):788–807.

[11] Leveque, R. J. (1999). *Numerical Methods for Conservation Laws.* Birkhauser Verlag, Basel Boston Berlin.

[12] P. Kachroo, L. R. and Sastry, S. (2014). Analysis of the godunov based hybrid model for ramp metering and robust feedback control design. *IEEE Transactions on Intelligent Transportation Systems*, 00:00.

[13] Trangenstein, J. (2008). *Numerical Solution of Hyperbolic Partial Differential Equations.* Cambridge University Press.

[14] V. J. Ervin, W. J. L. and Neda, M. (2007). Numerical analysis of a higher order time relaxation model of fluids. *International Journal of Numerical Analysis and Modeling*, 4.

[Wikipedia] Wikipedia. Coefficient of variation.

VITA

Graduate College
University of Nevada, Las Vegas

Puneet Lakhanpal

Home Address:
    604 Waterbury Ln
    Foster City, CA 94404

Degrees:

- Master of Science, Electrical and Computer Engineering, 2011
  University of Nevada, Las Vegas

- Bachelor of Technology, Electronics and Communication Engineering, 2009
  Indian Institute of Technology, Guwahati

Thesis Title:
    Numerical Simulations of Traffic Flow Models

Thesis Examination Committee:

- Chairperson, Monika Neda, Ph.D.

- Chairperson, Pushkin Kachroo, Ph.D., P.E.

- Committee Member, Hongtao Yang, Ph.D.

- Committeee Member, Amei Amei, Ph.D.

- Graduate Faculty Representative, Yingtao Jiang, Ph.D.